Mitochondrial exchanger NCLX plays a major role in the intracellular Ca2+ signaling, gliotransmission, and proliferation of astrocytes.

Parnis, J., Montana, V., Delgado-Martinez, I., Matyash, V., Parpura, V., Kettenmann, H., Sekler, I., Nolte, C.

This is the original version of the work, which was first published in:

Journal of Neuroscience
2013 Apr 24 ; 33(17): 7206-7219
doi: 10.1523/JNEUROSCI.5721-12.2013
Publisher: Society for Neuroscience

Cellular/Molecular

Mitochondrial Exchanger NCLX Plays a Major Role in the Intracellular Ca^{2+} Signaling, Gliotransmission, and Proliferation of Astrocytes

Julia Parnis,[1] Vedrana Montana,[3] Ignacio Delgado-Martinez,[1,5,6] Vitali Matyash,[1] Vladimir Parpura,[3,4] Helmut Kettenmann,[1] Israel Sekler,[2] and Christiane Nolte[1]

[1]Cellular Neurosciences, Max Delbrück Centre for Molecular Medicine, Berlin 13092, Germany, [2]Ben Gurion University, Beer-Sheva 84105, Israel, [3]Department of Neurobiology, University of Alabama, Birmingham, Alabama 35294, [4]Department of Biotechnology, University of Rijeka, 51000 Rijeka, Croatia, and [5]Department of Neurosurgery, Charité University Hospital, Berlin 10117, Germany, and [6]Singapore Institute of Neurotechnology (SINAPSE), Singapore 117456

Mitochondria not only provide cells with energy, but are central to Ca^{2+} signaling. Powered by the mitochondrial membrane potential, Ca^{2+} enters the mitochondria and is released into the cytosol through a mitochondrial Na^{+}/Ca^{2+} exchanger. We established that NCLX, a newly discovered mitochondrial Na^{+}/Ca^{2+} exchanger, is expressed in astrocytes isolated from mice of either sex. Immunoblot analysis of organellar fractions showed that the location of NCLX is confined to mitochondria. Using pericam-based mitochondrial Ca^{2+} imaging and NCLX inhibition either by siRNA or by the pharmacological blocker CGP37157, we demonstrated that NCLX is responsible for mitochondrial Ca^{2+} extrusion. Suppression of NCLX function altered cytosolic Ca^{2+} dynamics in astrocytes and this was mediated by a strong effect of NCLX activity on Ca^{2+} influx via store-operated entry. Furthermore, Ca^{2+} influx through the store-operated Ca^{2+} entry triggered strong, whereas ER Ca^{2+} release triggered only modest mitochondrial Ca^{2+} transients, indicating that the functional cross talk between the plasma membrane and mitochondrial domains is particularly strong in astrocytes. Finally, silencing of NCLX expression significantly reduced Ca^{2+}-dependent processes in astrocytes (i.e., exocytotic glutamate release, *in vitro* wound closure, and proliferation), whereas Ca^{2+} wave propagation was not affected. Therefore, NCLX, by meditating astrocytic mitochondrial Na^{+}/Ca^{2+} exchange, links between mitochondria and plasma membrane Ca^{2+} signaling, thereby modulating cytoplasmic Ca^{2+} transients required to control a diverse array of astrocyte functions.

Introduction

Ca^{2+} signaling is central for the regulation of astrocyte functions and for interastrocytic and astrocyte–neuron communication. Neuronal activity, via the activation of metabotropic receptors, triggers transient increases in the cytosolic Ca^{2+} concentration in astrocytes that leads to the release of gliotransmitters such as ATP and glutamate, which can signal to adjacent neurons (Agulhon et al., 2008; Perea et al., 2009). Astrocytic Ca^{2+} transients after metabotropic receptor activation are initiated by release of Ca^{2+} from the ER stores and by the entry from the extracellular space through store-operated Ca^{2+} channels. The spatiotemporal pattern of cytoplasmic Ca^{2+} signals is dynamically organized and allows for a great complexity of astrocytic Ca^{2+} responses.

Mitochondria, in addition to their metabolic role, participate in intracellular Ca^{2+} signaling via dynamic buffering and shuttling cytosolic Ca^{2+}. Powered by the mitochondrial membrane potential, Ca^{2+} enters mitochondria via the mitochondrial uniporter (Baughman et al., 2011; De Stefani et al., 2011; Pizzo et al., 2012) and is extruded from mitochondria via Na^{+}-dependent or -independent pathways (Drago et al., 2011). Mitochondria rapidly sense cellular Ca^{2+} signals and act as local Ca^{2+} buffers in the vicinity of Ca^{2+} release sites such as the ER or plasma membrane Ca^{2+} channels. By buffering and shuttling Ca^{2+}, they modulate local and bulk cytoplasmic Ca^{2+} changes (Szabadkai and Duchen, 2008; Contreras et al., 2010), thereby controlling cell-type-specific functions. Different cell types may vary with regard to mitochondrial Ca^{2+} handling, in particular Ca^{2+} extrusion mechanisms (Pizzo et al., 2012). At the neuronal synapse, for example, the mitochondrial Na^{+}/Ca^{2+} exchanger participates in shaping Ca^{2+} signals, thus modulating neuronal activity and synaptic plasticity (Kann and Kovács, 2007; Pizzo et al., 2012). Activity of the mitochondrial exchanger has also been documented in astrocytes, where it is closely linked to exocytotic release of

Received Dec. 11, 2012; revised Feb. 20, 2013; accepted Feb. 25, 2013.

Author contributions: V.P., H.K., I.S., and C.N. designed research; J.P., V. Montana, and I.S. performed research; I.D.-M. and V. Matyash contributed unpublished reagents/analytic tools; J.P., V. Montana, I.D.-M., V. Matyash, V.P., H.K., and I.S. analyzed data; J.P., V. Montana, V.P., H.K., I.S., and C.N. wrote the paper.

This work was supported by the German Israeli Foundation (Grant #917/2006 to I.S., C.N., and H.K.) and by the Hezneq faculty grant to I.S. I.D.M. was supported by the NeuroCure Cluster of Excellence (Charité University Hospital, Berlin). V.P. is supported by the National Science Foundation (Grant #CBET 0943343). We thank Prof. Michal Hershfinkel for helpful discussion and Regina Piske and Irene Haupt for excellent technical assistance.

The authors declare no competing financial interests.

Correspondence should be addressed to either of the following: Christiane Nolte, PhD, Cellular Neurosciences, Max Delbrueck Center for Molecular Medicine, Robert-Roessle-Strasse 10, 13125 Berlin, Germany, E-mail: cnolte@mdc-berlin.de; or Israel Sekler, PhD, Department of Physiology, Ben Gurion University, P.O. Box 653 Beer Sheva, 84105 Israel, E-mail: sekler@bgu.ac.il.

DOI:10.1523/JNEUROSCI.5721-12.2013

 0270-6474/13/337206-14$15.00/0

glutamate and mediates a robust cytosolic and mitochondrial Na^+ transport (Bernardinelli et al., 2006; Reyes and Parpura, 2008; Verkhratsky et al., 2012).

The benzothiazepine CGP37157 effectively blocks the activity of the mitochondrial exchanger. However, CGP37157, like other benzothiazepines, also modulates the activity of other Ca^{2+} channels and transporters that participate in glial Ca^{2+} signaling, among them SERCA, L-type, and the store-operated channels (Czyz and Kiedrowski, 2003; Thu le et al., 2006; Neumann et al., 2011). Molecular tools that selectively control the exchanger's activity or expression were not available because the identity of the mitochondrial exchanger gene was unknown. We have recently found that mitochondrial Na^+/Ca^{2+} exchange can be mediated by a member of the Na^+/Ca^{2+} exchanger superfamily, NCLX (Palty et al., 2010), and devised siRNA-based tools that control NCLX activity and thus can demonstrate its impact on mitochondrial and global cellular Ca^{2+} dynamics.

In the present study, we show that NCLX is the mitochondrial exchanger in astrocytes and plays a distinct role in controlling the ER- versus store-operated channel-dependent Ca^{2+} signals in astrocytes. By differentially controlling these Ca^{2+} signaling pathways, NCLX plays an essential role in facilitating a diverse array of astrocytic cellular activities ranging from release of glutamate to wound healing and proliferation.

Materials and Methods

Astrocyte cell culture

Procedures for animal work were approved by the Federal Ministry of Berlin (Landesamt für Gesundheit und Soziales) or the University of Alabama-Birmingham institutional animal care and use committee.

Enriched astrocyte cultures were prepared from cortices of 0- to 2-d-old newborn Naval Medical Research Institute mice or C57BL/6 mice of either sex, as described previously (Lyons and Kettenmann, 1998). Briefly, mice were killed by decapitation and cortical tissue was carefully freed from blood vessels and meninges, trypsinized, and gently triturated with a fire-polished pipette in the presence of 0.05% DNase (Worthington Biochem). After two washes, cells were cultured in DMEM with 10% fetal calf serum in Petri dishes (10 cm in diameter), in 25 cm^2 flasks, or on poly-L-lysine-coated glass coverslips at 37°C in a humidified 5% CO_2/95% air atmosphere. After 1 d, cells were washed twice with HBSS to remove cellular debris.

For glutamate release experiments and the associated subset of calcium-imaging experiments, astrocyte cultures were prepared from visual cortices of 0- to 2-d-old C57BL/6 mice of either sex as described previously (Reyes et al., 2011). Astrocytes were grown in culture medium containing α-MEM without phenol red (Invitrogen) supplemented with fetal bovine serum (10% v/v; Thermo Scientific Hyclone), L-glutamine (2 mM), D-glucose (20 mM), sodium pyruvate (1 mM), penicillin (100 I.U./ml), streptomycin (100 μg/ml), and sodium bicarbonate (14 mM), pH 7.35. After 7–18 d in culture, cells were purified for astrocytes (>99% for the astrocytes from visual cortices). In some cases, after the purification procedure, astrocytes were returned to the incubator up to 1 d before transfection.

Reagents and plasmids

CGP37157 (7-chloro-5-(2-chlorophenyl)-1,5-dihydro-4,1-benzothiazepin-2(^3H)-one; Ascent Scientific) was freshly prepared before each experiment at a stock concentration of 40 mM in DMSO and was used at a final concentration of 20 μM. ATP and all other reagents were obtained from Sigma-Aldrich.

The plasmid expressing mitochondrial-targeted ratiometric-pericam (pcDNA3.1$^+$-mtRP) was kindly provided by Atsushi Miyawaki (Wako, Japan). Double-stranded ON-TARGETplus SMARTpool siRNAs, used to silence NCLX expression, and siGLO RISC-Free siRNA were obtained from Dharmacon or Thermo Fisher Scientific.

Transfection procedures

For silencing NCLX expression, astrocytes were transfected with an ON-TARGET mixture of siRNAs (siNCLX) or a pool of control ON-TARGETplus nontargeting siRNAs (siControl) at a final concentration of 10 nM siRNA. As additional controls, in some experiments, cells were treated only with a transfection reagent (mock-treated) or untreated. Astrocytes were analyzed 3 d after the transfection. Lipofectamine RNAiMAX (1 μl/1200 μl of medium; Invitrogen) or TransIT-TKO (6 μl/flask containing 4 ml of medium;Mirus) was used to transfect astrocytes with siRNA. The fluorescent transfection marker siGLO RISC-Free siRNA was used in the cytoplasmic Ca^{2+}-imaging experiments and glutamate release experiments to identify siRNA-transfected cells. Analysis of siGLO fluorescence, visualized using a standard tetramethylrhodamine isothiocyanate filter set (Chroma Technology), indicated that siRNA was delivered to all astrocytes and retained intracellularly throughout the duration of experiments.

To determine mitochondrial Ca^{2+} responses after knock-down of NCLX expression in astrocytes, the siNCLX or control siRNAs (siControl) were cotransfected with pcDna3.1$^+$-mtRP (1 μg) using Lipofectamine 2000 (1 μl/each 300 μl of medium; Invitrogen) according to the manufacturer's protocol. Transfection efficiency was ~1–5%. Mitochondrial expression of the pericam sensor mtRP was documented in a two-photon laser scanning microscope (Till Photonics) equipped with a water-immersion objective (40×, numerical aperture [NA] 0.8; Olympus). mtRP was excited by a Chameleon Ultra II laser (Coherent) set to a wavelength of 920 nm, and *z*-stacks of 150 × 150 μm images with a step size of 2 μm were acquired.

Cell fractionation and Western blot analysis

Cell/tissue lysis. Astrocytic monolayers or homogenized total brains were lysed with RIPA buffer (Sigma-Aldrich) supplemented with protease inhibitors (Roche Diagnostics), agitated at 4°C for 30 min, and centrifuged for 20 min at 14,000 rpm. The supernatants were then collected and frozen at −70°C until use.

Subcellular fractionation. ER, cytosol, and mitochondria-enriched fractions from primary astroglia cultures were obtained as described previously (Bozidis et al., 2007). Briefly, ~$4–5 \times 10^7$ cells were washed once with PBS, suspended in MTE solution (270 mM D-mannitol, 10 mM Tris, 0.1 mM EDTA, pH 7.4), and then lysed by sonication. The homogenate was centrifuged at 1400 × g for 10 min and the supernatant (total fraction) was recovered and further centrifuged for 10 min at 15,000 × g. The resulting pellet (crude mitochondria) and supernatant (crude ER) were separated for further purification, loaded on the top of a sucrose gradient, centrifuged, isolated, and washed once. Pellets were resuspended in PBS and frozen at −70°C until use.

The plasma-membrane-enriched fraction was purified using a cell surface protein isolation kit (Pierce/Thermo Fisher Scientific) according to the manufacturer's instructions.

Protein quantification and immunoblotting. Protein concentration was determined using the BCA assay (Pierce/Thermo Fisher Scientific). First, the plasma-membrane-enriched fraction was dialyzed 3 times in 2 L of PBS and then assayed using the BCA method. Extracted proteins (20 μg/lane) were separated on 10% or 12% SDS-PAGE and transferred onto polyvinylidene difluoride membrane (GE Healthcare Europe). Membranes were probed using the following antibodies: polyclonal anti-NCLX (1:1000; Palty et al., 2004), anti-GAPDH (1:10,000; New England Biolabs), anti-ANT (1:100; Santa Cruz Biotechnology), anti-Sec62 (1:1000; kindly provided by Prof. Dr. T. Sommer, Max Delbrück Center for Molecular Medicine, Berlin), and anti-*N*-cadherin (1:1000; BD Biosciences).

Real-time quantitative RT-PCR

Efficacy of silencing was determined by real-time quantitative RT-PCR analysis, which was performed 3 d after the delivery of siRNA (as described above). Astrocytes were harvested and total RNA was extracted with the InviTrap Spin universal mini kit (Invitek) according to the manufacturer's instructions. This was followed by first-strand cDNA synthesis using the SuperScript II reverse transcriptase enzyme (Invitrogen) with 1 μg of total RNA and oligo-dT primers. Quantitative RT-PCR

was performed with gene-specific assays purchased from Dharmacon/Thermo Fisher Scientific) according to the manufacturer's instructions. GAPDH served as the internal control to quantify relative changes in gene expression.

Glutamate measurements in stimulated solitary astrocytes

Stimulation of astrocytes. To evoke an increase in cytosolic Ca^{2+} of solitary astrocytes and consequential exocytotic glutamate release, we mechanically stimulated astrocytes using glass pipettes filled with external solution as described in detail previously (Hua et al., 2004). This approach has physiological relevance and allows spatiotemporal control of the stimulus application without affecting plasma membrane integrity (Hua et al., 2004; Malarkey and Parpura, 2011). To control for the contact between the pipette and the solitary astrocyte, we monitored pipette resistance using a patch-clamp amplifier (PC-ONE; Dagan). The strength of the stimulus, measured as the increase in the pipette resistance upon establishment of a pipette-astrocyte contact, was comparable under all conditions tested (Mann–Whitney *U* test, $p = 0.27–0.34$).

Glutamate measurements. Ca^{2+}-dependent glutamate release from cultured solitary astrocytes was measured using the L-glutamate dehydrogenase (GDH)-linked assay as described previously (Hua et al., 2004; Montana et al., 2004; Lee et al., 2008). Astrocytes were bathed in an enzymatic assay solution containing external solution supplemented with NAD^+ (1 mM, catalog #N6522; Sigma-Aldrich) and GDH (~53–137 IU/ml, catalog #G2626; Sigma-Aldrich, pH = 7.4). External solution contained the following (in mM): 140 NaCl, 5 KCl, 2 $CaCl_2$, 2 $MgCl_2$, 5 glucose, and 10 HEPES, pH 7.4. When released to the extracellular space, glutamate gets converted by GDH to α-ketoglutarate with the concomitant reduction of the bath supplied coenzyme NAD^+ to NADH, the latter being a fluorescent product when excited by UV light. Visualization was achieved at room temperature (20–24°C) using a standard DAPI filter set (Nikon). Every experiment was preceded by a sham run on astrocytes bathed in solution lacking GDH and NAD^+ for photobleaching and background subtraction calculation. After correction, all imaging data were expressed as dF/F_0 (%), where *dF* represents the change of fluorescence and F_0 represents the background fluorescence level surrounding the solitary astrocyte, immediately and laterally of its soma, before mechanical stimulation. Imaging acquisition for these experiments is described below as Ca^{2+} measurements in solitary astrocytes.

Fluorimetric measurements of cytosolic and mitochondrial Ca^{2+}

Cytosolic Ca^{2+} levels in astrocytes were recorded using the Ca^{2+} indicators fura-2 AM or fluo-3 AM as described previously (Hua et al., 2004; Montana et al., 2004; Lee et al., 2008). Subconfluent astrocytic monolayers on coverslips were loaded for 30 min at room temperature with 2.5 μM fura-2 AM (Invitrogen) in external solution (HEPES buffer; see below), followed by at least a 20 min wash to allow de-esterification. Alternatively, solitary astrocytes were loaded with fluo-3 AM (1 μg/ml; Invitrogen) in external solution containing pluronic acid (0.025% w/v; Invitrogen) for 20 min at room temperature, followed by washing in external solution for 20 min at room temperature. Mitochondrial Ca^{2+} levels were monitored in astrocytes transiently expressing mtRP. All Ca^{2+}-imaging experiments were performed at room temperature. Cells were transferred to the stage of an Axiovert 135 inverted microscope (Carl Zeiss) equipped with a cooled CCD camera (PCO Imaging) and a Polychrome V monochromator (TILL Photonics) and superfused with 3.5–4.0 ml/min Ca^{2+}-full HEPES buffer containing the following (in mM): NaCl 150.0, KCl 5.4, $MgCl_2$ 1.0, $CaCl_2$ 2.0, HEPES 10.0, and glucose 10.0, pH 7.4). In Ca^{2+}-free HEPES buffer, 2 mM Ca^{2+} was replaced by 2 mM $MgCl_2$ and 0.5 mM EGTA. Images were acquired through a 20× objective for cytoplasmic-imaging experiments using Axon Imaging Workbench 6 software (INDEC BioSystems) at an acquisition rate of 1 frame/1.2 s. Fura-2 AM-loaded cells were excited at wavelengths of 340 and 380 nm and the emitted light passed through a long-pass emission filter at 510 (± 40) nm.

Mitochondrial Ca^{2+} levels were monitored in cells transiently expressing mtRP using a 40× objective at an excitation wavelength of 430 nm (Ca^{2+}-sensitive wavelength; Nagai et al., 2001) and 480 nm, presented as F_0/F_{430} or R/R_0 ($r = F_{480}/F_{430}$). In some of the indicated experiments described in the Results section, cell data were taken only at 430 nm because of significant fluorescence changes at 480 nm, likely related to changes in mitochondrial pH_i (Malli et al., 2003). When excited at 480 nm, mitochondrial pericam mtRP is strongly affected by pH, and the excitation of mtRP at 480 nm was in fact previously used effectively for monitoring mitochondrial pH changes (Jiang et al., 2009). Emitted light of cells excited in either wavelength was collected using a 535 nm bandpass filter. F_0 was calculated as the average value obtained during the 50–100 s before the stimulus application.

Cytoplasmic Ca^{2+} measurements in solitary astrocytes (associated with glutamate measurements) were performed on an inverted microscope (TE 300; Nikon) equipped with differential interference contrast and wide-field fluorescence illumination (halogen and xenon arc lamps, respectively). Visualization of fluo-3 AM was accomplished using a standard FITC filter set (Chroma Technology). Images were captured through a 40× fluor objective (NA 1.3; Nikon) using a CoolSNAP-HQ cooled charge-coupled device camera (Photometrics) driven by V++ imaging software (Digital Optics). For time-lapse image acquisition, a camera and an electronic shutter (Vincent Associates) inserted in the excitation pathway were controlled by the software. All imaging data were background subtracted using regions of the coverslip field containing no cells. Data are expressed as $dF/F_0 \pm$ SEM (%) in which *dF* represents the change of fluorescence and F_0 represents the fluorescence of the cell soma at rest.

Cell viability and nuclear staining

To test the effects that transfection agents and downregulation of NCLX may have on viability of astrocytes, we assessed the ability of these cells to accumulate the vital stain calcein (Hua et al., 2004). Cultured astrocytes were incubated with calcein AM (1 μg/ml; Invitrogen) and pluronic acid (0.025% w/v) in complete culture medium at 37°C in a humidified 5% CO_2/95% air atmosphere for 10 min. De-esterification of calcein AM was permitted for 10 min by keeping astrocytes in external solution at room temperature. During the last 5 min, nuclei were stained by adding the cell permeant nuclear stain Hoechst 33342 (5 μg/ml; Invitrogen). Calcein was visualized using the FITC filter set, and a DAPI filter set was used for visualization of Hoechst. Image acquisition and processing was done as reported above, except here we used a 60× Plan Apo oil-immersion objective (1.4 NA; Nikon).

Astrocytic wound-healing assay

Astrocytic wound healing was evaluated using a scratch assay described previously (Gebäck et al., 2009). One day after seeding into 4-well plates, semiconfluent astrocytes were transfected with either 10 nM siNCLX-silencing RNA, siControl or mock-transfected as described, or left untreated and cultured for 3 d to reach full confluence. At day 4, astrocytic monolayers were scratched with a 200 μl sterile pipette tip in the shape of a horizontal double cross (Fig. 7*B*). After two washes with PBS to remove detached cells and debris, cells were incubated in serum-reduced medium containing 1% FBS. Phase contrast images of the wounds were acquired at 0–72 h after scratching using a 5× magnification objective and frame grabber software (InteQ). At each acquisition time point, the culture dish and the cross-shaped wound area was exactly centered and images were acquired at identical positions (Fig. 7*A*,*B*). TScratch software (Gebäck et al., 2009; www.cse-lab.ethz.ch/software) was used to determine the percentage area without cells at different time points (open wound area). The final time point was defined as the time point when the initial open wound area was closed by at least two-thirds (in untreated control). At least six replicates per condition were analyzed and the results are expressed as the percentage open wound area.

Cell proliferation assay

Astrocyte proliferation was determined by a colorimetric immunoassay measuring 5-bromodeoxyuridine (BrdU) incorporation (Roche Diagnostics) in proliferating cells. Two days after transfection of astrocytes with siRNA, cells were trypsinized and seeded into 96-well plates at a density of 3.5×10^3 cells/well. One day after the transfection, medium was changed to medium containing 1% FCS and BrdU was added 3 d after the transfection according to the manufacturer's instructions. The

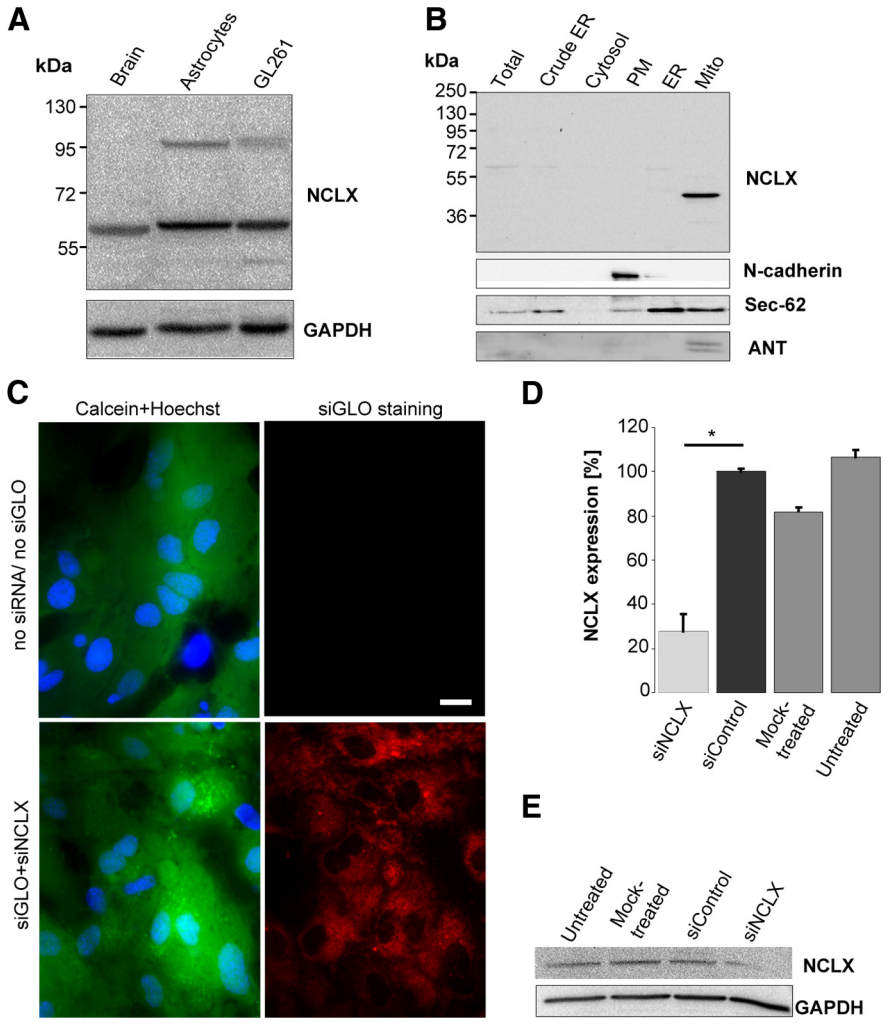

Figure 1. ***A***, immunoblot analysis of NCLX expression in brain extracts of newborn mice, primary murine astrocytes, and the murine astrocytoma cell line GL261 (top). GAPDH serves as an internal loading control (bottom). ***B***, NCLX is enriched in the mitochondria of astrocytes. NCLX expression in indicated cellular compartments: total, crude ER, cytosol, plasma membrane (PM), ER, and mitochondria (Mito)-enriched fractions (top). The membranes were stripped and reprobed for PM (N-cadherin), ER (Sec-62), and mitochondrial (ANT) markers (bottom). ***C***, Astrocytes are viable after 100% efficient siRNA transfection. Top row shows untreated control astrocytes (no siRNA); bottom row shows astrocytes treated with siGLO and siNCLX (siGLO + siNCLX). Left: Astrocytes accumulated calcein (green), indicating their viability. Nuclei are marked with Hoechst 33342 in blue. Right: Red fluorescence of the same area; untreated astrocytes display dim autofluorecence, whereas siRNA (siGLO + SiNCLX)-treated cells show punctate stain, consistent with intracellular accumulation of the transfection marker siGLO. Scale bar, 20 μm. ***D***, Quantitative RT-PCR analysis after cotransfection with mtRP and siNCLX or siControl, respectively. Untreated and mock-treated (tranfection agent only) cells were used as additional controls. Experiment was performed four times, each in triplicate. Values are given as means with SEM (*$p < 0.05$, Wilcoxon-Mann–Whitney *U* test). ***E***, Immunoblot analysis showing NCLX expression in untreated and mock-treated astrocytes, or transfected with siControl or siNCLX (top). GAPDH serves as an internal loading control (bottom).

assay was performed 24 h after the addition of BrdU according to the manufacturer's instructions with five replicates for each condition.

Astrocytic Ca^{2+} waves

Confluent astrocytes grown on coverslips were loaded with 5 μm fluo-4 AM for 30 min at room temperature. After dye loading and washing, the coverslips were mounted in the bath containing HEPES buffer, and Ca^{2+} waves were evoked mechanically by touching a single astrocyte with a micropipette (Cornell-Bell et al., 1990). The changes in fluo-4 AM fluorescence were acquired with 10× Plan objective (Carl Zeiss) at an acquisition speed of 1 frame/1.2 s.

Data analysis

The rate of Ca^{2+} influx (entry) or efflux was obtained by measuring the initial slope of Ca^{2+} rise or decline, respectively, as illustrated in Fig. 2*D*, *E*, insets. The maximal value of the normalized fluorescence intensity was taken as the peak amplitude or influx. To evaluate the response time, we determined the width of the peak at its half-amplitude. The cumulative fluorescence resulted from the area under the curve and was derived by integration. Data analysis was performed with MS Excel 2003, Origin 7, KaleidaGraph version 4.1, and ImageJ software.

For the glutamate release analysis, the dF/F_0 values of the test group (siNCLX) were ranked and normalized to siControl to allow comparisons between experimental batches and to accommodate for variations in GDH concentration and culture conditions. In associated experiments, similar ranking of $Ca^{2+}{}_{cyt}$ dF/F_0 was done for consistency. Resulting proportions are expressed as means ± SEM. Data analysis was performed with MS Excel 2003, GB-Stat, and V++ imaging software (Digital Optics).

A custom-made algorithm programmed in C++ was used to calculate the Ca^{2+} wave velocity at which the wave reached each cell. For this purpose, two parameters were determined; (1) the time at which the increase in cytoplasmic Ca^{2+} was observed in a given cell and (2) the distance of this cell from the stimulation point. The first parameter was measured by a peak detection algorithm in the derivative of the mean intensity values over time in the labeled regions. Cell detection was done by first obtaining a binary mask of the SD projection of the time stack using automatic triangle thresholding (Zack et al., 1977). Individual cells were identified thereafter by a two-pass connected-component labeling (Shapiro and Stockman, 2001).

Statistics

All experiments were done at least three times using astrocytic cultures originating from independent cell preparations. Data are presented as mean with SEM for column graphs, with exception of Figure 3, where we used box plots with median, interquartile range (25th and 75th percentiles), and minimum and maximum values (whiskers). For the parametrical data, the statistical significance was evaluated using Student's *t* test, unpaired and double-tailed. For the experiments with more than two test groups to compare, a multiple parameter one-way ANOVA test was used followed by Bonferroni posttest. For the comparison of nonparametric data, a Mann–Whitney *U* test or Kruskall–Wallis test followed by Bonferroni correction and Mann–Whitney *U* test pair comparisons were used to evaluate the statistical significance (*$p < 0.05$; **$p < 0.01$; ***$p < 0.001$).

Results

NCLX is enriched in the mitochondria of astrocytes

Recently, NCLX has been identified as the mitochondrial Na^+/Ca^{2+} exchanger in several cell types (Palty et al., 2010; Kim et al., 2012). To determine whether NCLX is the mitochondrial exchanger in astrocytes, we first evaluated NCLX expression in lysates from cultures of cortical astrocytes by Western blot analysis. Consistent with the previous studies (Palty et al., 2010), a major band of ~60 kDa and a fainter band at ~100 kDa related to the SDS-stable NCLX dimer were detected. The 60 kDa band was also detected in brain lysates from newborn

mice and in an astrocytoma cell line GL261, whereas the 100 kDa band was not detectable in brain homogenate, but was present in GL261 cells (Fig. 1*A*).

To analyze NCLX expression in different cellular compartments, we performed subcellular fractionation of cultured astrocytes and determined NCLX expression using Western blot analysis. The fractions were counterstained with organelle-specific markers (Fig. 1*B*) to determine the separation quality of the fractions. Total, crude ER, and ER-enriched fractions revealed a faint band at ~60 kDa, whereas no band was visible in the plasma membrane or cytosolic fractions. Interestingly, the mitochondrial fraction showed a strong NCLX-positive band of slightly reduced molecular weight (MW), suggesting that the passage of NCLX to the mitochondria may be linked to posttranslational proteolysis. Probing with anti-ANT and anti-*N*-cadherin antibodies showed a good separation of the mitochondrial and plasma membrane fractions, respectively. Some degree of ER cross-contamination was detected in other fractions when probing the ER marker Sec-62, which is likely related to the physical cross-linking of the ER with other organelles. Nonetheless, these data show that the astrocytic Na^+/Ca^{2+} exchanger NCLX is primarily located in mitochondria.

Molecular silencing of NCLX in astrocytes

To assess the role of NCLX in modulating astrocytic Ca^{2+} signaling and related functions, the expression of the exchanger was knocked down with an NCLX-specific mixture of siRNAs (siNCLX). The fluorescently tagged siRNA siGLO was used as a cotransfection marker to determine optimal conditions for effective NCLX silencing and to detect transfected cells; calcein live cell staining was applied to assess cell viability (>99%). Cells treated with siRNA (siGLO + siNCLX) showed punctate red staining, consistent with intracellular accumulation of the transfection marker siGLO (Fig. 1*C*, lower right). siGLO fluorescence was visible in all treated viable cells, showing that cells were successfully transfected. The untreated cells showed only dim autofluorescence (Fig. 1*C*, upper right). All astrocytes showed a similar accumulation of calcein regardless of whether they were treated with siRNA or were untreated controls (Fig. 1*C*, left column), indicating that the siRNA transfection procedure did not affect cell viability.

The efficiency of NCLX silencing via siRNA was assessed by quantitative RT-PCR. Optimal NCLX gene silencing via siRNA was achieved after 3 d using 10 nM siNCLX. NCLX expression in the presence of siNCLX was reduced to 24.9 ± 1.3% of the expression level seen in astrocytes transfected with siControl (Fig. 1*D*, $n = 4$ experiments, $^*p < 0.05$). NCLX mRNA expression levels remained almost unchanged in cells treated only with the transfection agent (mock-treated) and in untreated control cells (84.0 ± 13.9% and 101.7 ± 4.5%, respectively). Consequently, all experiments were performed on astrocytic cultures 3 d after siRNA treatment.

NCLX silencing on mRNA level also affected the expression of the NCLX protein. Western blot analysis of astrocytic extracts showed a reduction in NCLX expression in astrocytes transfected with siNCLX compared with astrocytes transfected with siControl, mock-treated, or untreated cells (Fig. 1*E*).

NCLX conducts mitochondrial Ca^{2+} efflux in astrocytes

To monitor mitochondrial Ca^{2+} responses, primary astrocytes were transfected with mtRP (Nagai et al., 2001) Expression of mtRP reached maximal intensity ~48–72 h after transfection. mtRP expression pattern manifested a typical network-like mitochondrial distribution consistent with the strict mitochondrial localization of this Ca^{2+} reporter (Fig. 2*A*). Resting mitochondrial Ca^{2+} levels in astrocytes transfected with siNCLX were higher than values obtained from mitochondria of astrocytes treated with control siRNA (Fig. 2*B*). Application of ATP (100 μM) to astrocytes in Ca^{2+}-free HEPES Ringer's solution for 100 s elicited a fast rise in the mitochondrial Ca^{2+} corresponding to the Ca^{2+} uptake phase followed by a slower efflux (Fig. 2*C*, $n = 10$ and 11 experiments for siControl and siNCLX-transfected astrocytes, respectively). Mitochondrial Ca^{2+} influx and efflux rates were determined as described in Materials and Methods and as indicated in Fig. 2*D*,*E*, insets. Comparison of the efflux rates of the ATP-elicited mitochondrial Ca^{2+} responses in siNCLX-treated versus siControl-treated cells showed that the mitochondrial efflux rate was decreased by 60.2% in siNCLX-treated cells compared with siControl astrocytes (from $15.1 \pm 1.5 \times 10^{-4}$/s to $6.0 \pm 0.6 \times 10^{-4}$/s, $n = 10$ and 11 experiments and $n = 38$ and 64 regions for siControl and siNCLX conditions, respectively, $^{***}p < 0.001$; Fig. 2*D*). Moreover, silencing of NCLX significantly increased the net mitochondrial Ca^{2+} influx by 28.1% compared with the siControl condition (from $8.7 \pm 0.6 \times 10^{-2}$ to $11.1 \pm 0.7 \times 10^{-2}$; $n = 10$ and 11 experiments with siControl- and siNCLX- transfected astrocytes, respectively, $^*p < 0.05$; Fig. 2*E*).

The effect of NCLX activity on mitochondrial Ca^{2+} fluxes was also evident when we used the pharmacological inhibitor of mitochondrial Na^+/Ca^{2+} exchange; application of 20 μM CGP37157 resulted in a 62.4% reduction of the ATP-induced mitochondrial Ca^{2+} efflux in treated astrocytes compared with cells treated with vehicle (DMSO) (control, $6.4 \pm 0.5 \times 10^{-4}$/s, $n = 15$ experiments and 106 regions of interest; CGP37157-treated group, $2.5 \pm 0.5 \times 10^{-4}$/s, $n = 11$ experiments and 75 regions of interest, $^{***}p < 0.001$; Fig. 2*F*,*G*). The average net mitochondrial Ca^{2+} influx was increased from $8.6 \pm 0.4 \times 10^{-2}$/s to $12.5 \pm 0.9 \times 10^{-2}$/s in the presence of CGP37157 ($n = 15$ and 11 experiments with control- and CGP37157- treated astrocytes, respectively, $^*p < 0.05$; Fig. 2*H*).

NCLX inhibition, either by specific molecular silencing or by the pharmacological inhibitor, significantly reduced mitochondrial Ca^{2+} extrusion, thereby also indirectly increasing the net Ca^{2+} influx. These data indicate that NCLX mediates mitochondrial Ca^{2+} efflux in astrocytes and thereby shapes the mitochondrial Ca^{2+} transients.

NCLX shapes the ATP-induced cytosolic Ca^{2+} response in astrocytes

Mitochondrial Ca^{2+} transport participates in intracellular Ca^{2+} signaling (Hoth et al., 1997; Hajnóczky et al., 1999; Malli et al., 2003; Parekh, 2008). Our finding that NCLX is the mitochondrial Na^+/Ca^{2+} exchanger in astrocytes provides us with a molecular basis to evaluate how mitochondria respond to or shape cytosolic Ca^{2+} responses in astrocytes and to determine the role of NCLX in this process. Astrocytes were cotransfected with siControl or siNCLX together with the transfection marker siGLO red. After 3 d, cells were loaded with fura-2 AM and cytoplasmic Ca^{2+} signals in response to application of 100 μM ATP were monitored from siGLO-red-positive cells, either in Ca^{2+}-containing buffer (Fig. 3*A–D*) or Ca^{2+}-free buffer (Fig. 3*E–H*). As described previously (Kresse et al., 2005), application of ATP in Ca^{2+}-containing buffer evoked a rapid increase of cytosolic Ca^{2+} mainly due to $InsP_3$-receptor-mediated release of Ca^{2+} from the ER stores, followed by an initial rapid decline and a slower decaying phase. The latter "elevated Ca^{2+} plateau" has been associated

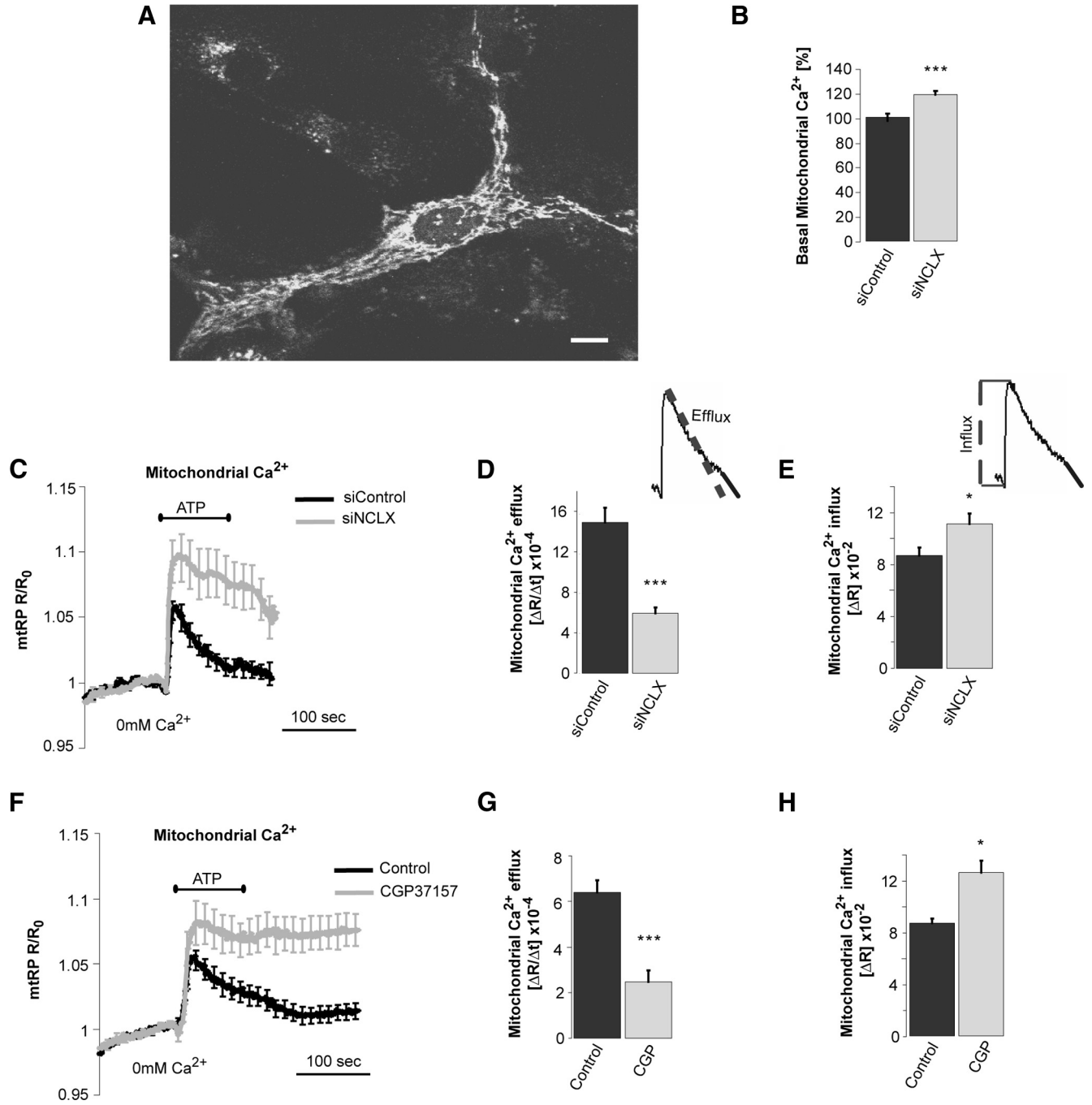

Figure 2. NCLX mediates mitochondrial Ca^{2+} efflux in astrocytes. ***A–E***, Primary astrocytes were cotransfected with mtRP and siNCLX or siControl and were analyzed after 3 d. ***A***, Two-photon microscopy image of astrocytes transfected with mtRP reveals typical mitochondrial pattern of the fluorescent pericam sensor. Scale bar, 10 μm. ***B–E***, Mitochondrial Ca^{2+} imaging. ***B***, Resting mitochondrial Ca^{2+} levels of astrocytes transfected with siNCLX- or control siRNA, R/R_0 values were determined from fluorescent mtRP imaging before application of the stimulus and normalized to the control condition ($n = 5$ cultures, $n = 134$ and 118 regions), ***C***, Mitochondrial Ca^{2+} signals of control and siNCLX-transfected astrocytes; 100 μM ATP in Ca^{2+}-free HEPES buffer was applied as indicated, averaged curves ± SEM. ***D–E***, Average rates of the mitochondrial Ca^{2+} efflux (slopes; ***D***) and influx (amplitudes, ***E***) in siControl and siNCLX-transfected astrocytes, comparing $n = 10$ ($n = 38$ regions) and $n = 11$ ($n = 64$ regions) experiments for each condition (***$p < 0.001$, *$p < 0.05$, Wilcoxon, Mann–Whitney U test). ***F–H***, Effect of CGP37157 on mitochondrial Ca^{2+} efflux. ***F***, Mitochondrial Ca^{2+} signals from control and CGP37157 (CGP)-treated astrocytes. Cells were superfused with Ca^{2+}-free HEPES buffer ± 20 μM CGP37157and 100 μM ATP was applied as indicated; shown are averaged curves ± SEM. ***G–H***, average rates of mitochondrial efflux (***G***) and influx (***H***). Values are given as means with SEM for $n = 15$ ($n = 106$ regions) and $n = 11$ ($n = 75$ regions) control and CGP37157 experiments, respectively (***$p < 0.001$, *$p < 0.05$, Wilcoxon, Mann–Whitney *U* test).

with Ca^{2+} influx from the extracellular space via store-operated Ca^{2+} entry (SOCE). The averaged Ca^{2+} transients indicate that the amplitude of the elevated Ca^{2+} plateau is reduced in NCLX-silenced astrocytes (Fig. 3*A*, $n = 12$ and 11 experiments for siControl and siNCLX-transfected astrocytes, respectively). To quantify the effect of NCLX silencing on the cytosolic Ca^{2+} transient, we determined the cumulative fura-2 AM fluorescence, peak amplitude, and half-amplitude time in siControl-treated versus siNCLX-treated astrocytes. The cumulative fluorescence was reduced by 39.3% in NCLX-silenced astrocytes (Fig. 3*B*), whereas the peak amplitude was reduced by 13.4% (Fig. 3*C*) and the half-amplitude time of the signal was reduced by 9.8% (Fig.

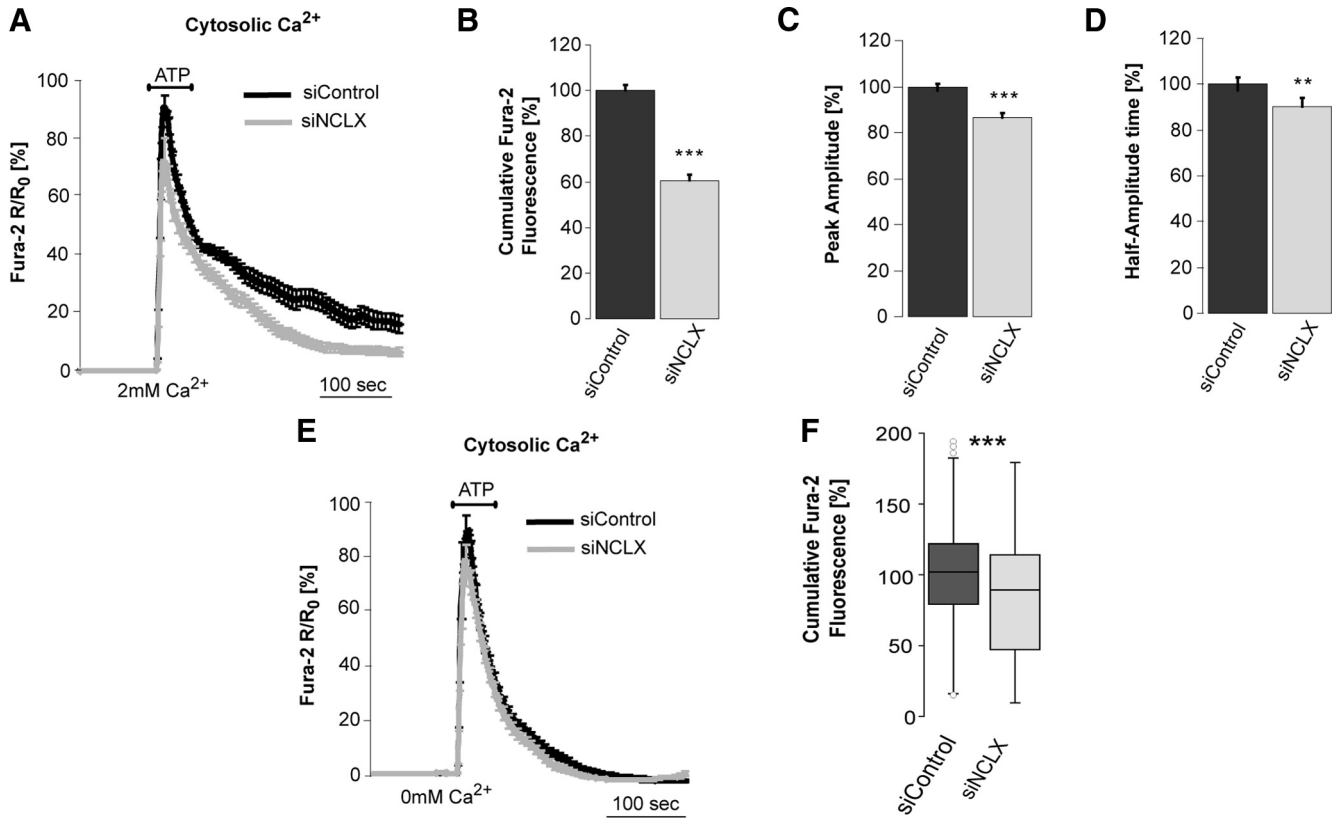

Figure 3. NCLX modulates ATP-induced Ca^{2+} responses in astrocytes. Primary astrocytes were cotransfected with siControl or siNCLX and siGLO red indicator. Cells were loaded with fura-2 AM and changes in cytoplasmic Ca^{2+} signals were monitored from siGLO-red-positive cells. ***A***, ***E***, Recording of average fura-2 AM fluorescence for control and siNCLX-transfected astrocytes in Ca^{2+}-containing buffer (***A***) and Ca^{2+}-free buffer (***E***); 100 μM ATP was added as indicated, averaged curves SEM. ***B–D***, Statistical analysis of the recordings shown in ***A***: cumulative response (***B***), amplitudes (***C***), and half-amplitude time (***D***) of the ATP-evoked Ca^{2+} responses. Values are given as mean with SEM ($n = 12$ experiments, $n = 294$ cells for control, and $n = 11$ experiments, $n = 222$ cells for siNCLX-transfected astrocytes, respectively; $^{***}p < 0.001$, $^{**}p < 0.01$, Wilcoxon, Mann–Whitney *U* test). ***F***, Box-plot chart of the cumulative Ca^{2+} responses corresponding to recordings in ***E*** indicating median (dark line), interquartile range (box), and minimum and maximum of the values (whiskers) ($^{***}p < 0.001$, Wilcoxon, Mann–Whitney *U* test).

3*D*) in NCLX-silenced astrocytes compared with siControl-treated astrocytes ($n = 12$ and 11 experiments, $n = 294$ siControl and $n = 222$ siNCLX-transfected astrocytes; $^{***}p < 0.001$, $^{**}p < 0.01$).

To determine the contribution of mitochondrial NCLX to the modulation of Ca^{2+} signals that originate from ER stores, we superfused cells with Ca^{2+}-free buffer and measured ATP-induced cytosolic Ca^{2+} signals in NCLX-silenced and siControl astrocytes. ATP triggered a fast rise followed by a fast decline of the cytoplasmic Ca^{2+} signal as described above. The elevated plateau phase, seen in Ca^{2+}-containing buffer (above) was, as expected, reduced under Ca^{2+}-free conditions. Knock-down of NCLX revealed a slight but significant reduction of the mean cumulative Ca^{2+} signal in NCLX-silenced astrocytes, with medians shifted from 102.1% in the siControl population to 89.4% in the NCLX-silenced astrocytes ($^{***}p < 0.001$; Fig. 3*F*). The representation of cumulative Ca^{2+} responses as median and interquartile ranges revealed that NCLX silencing is more pronounced in the lower quartiles of the data (25th percentile of the box plot): in those cells with overall lower cumulative Ca^{2+} responses, the shift was from 79% in the nonsilenced condition to 47.4% after NCLX knock-down (Fig. 3*F*).

These results indicate that stimulus-induced cytoplasmic Ca^{2+} signals in astrocytes, in particular those caused by the entry of Ca^{2+} from the extracellular space versus Ca^{2+} release from the ER store, are distinctly modulated by the activity of the mitochondrial Na^{+}/Ca^{2+} exchanger NCLX.

NCLX activity modulates the store-operated Ca^{2+} entry in astrocytes

SOCE is an important Ca^{2+} influx pathway in nonexcitable cells such as astrocytes (Kresse et al., 2005; Pivneva et al., 2008; Verkhratsky et al., 2012). Observations in other cell types showing that the mitochondrial Ca^{2+} shuttling machinery is essential to sustaining the activity of SOCE (Hoth et al., 1997; Malli et al., 2003; Parekh, 2008, and the reduction of the Ca^{2+}-elevated plateau phase seen in the ATP-induced Ca^{2+} signal in NCLX-silenced astrocytes (described above) prompted us to determine the specific influence of mitochondrial NCLX on Ca^{2+} influx through the SOCE pathway in astrocytes.

To quantify SOCE activity, we used a previously described protocol. Briefly, ER stores were depleted by application of ATP in the absence of extracellular Ca^{2+}. Cells were then superfused with Ca^{2+}-containing buffer, which resulted in a Ca^{2+} influx due to SOCE activity (Kresse et al., 2005; Fig. 4*A*). The amplitude of SOCE response measured at the steady phase was decreased from 100.0 ± 5.1% to 59.9 ± 3.1% after silencing of NCLX ($n = 9$ experiments; $n = 175$ and 131 cells for siControl and siNCLX-transfected astrocytes, respectively, $^{***}p < 0.001$; Fig. 4*B*). Moreover, the SOCE rate (reflected by the slope of the influx phase) was reduced from 100.0 ± 3.6% to 68.0 ± 3.7% by NCLX silencing ($^{***}p < 0.001$; Fig. 4*C*). A similar impairment on SOCE function was found in astrocytes superfused with 20 μM CGP3715. The drug reduced SOCE amplitude by 25.5% and the SOCE rate by 34.2% compared with vehicle-treated control ($n = 8$ and 7

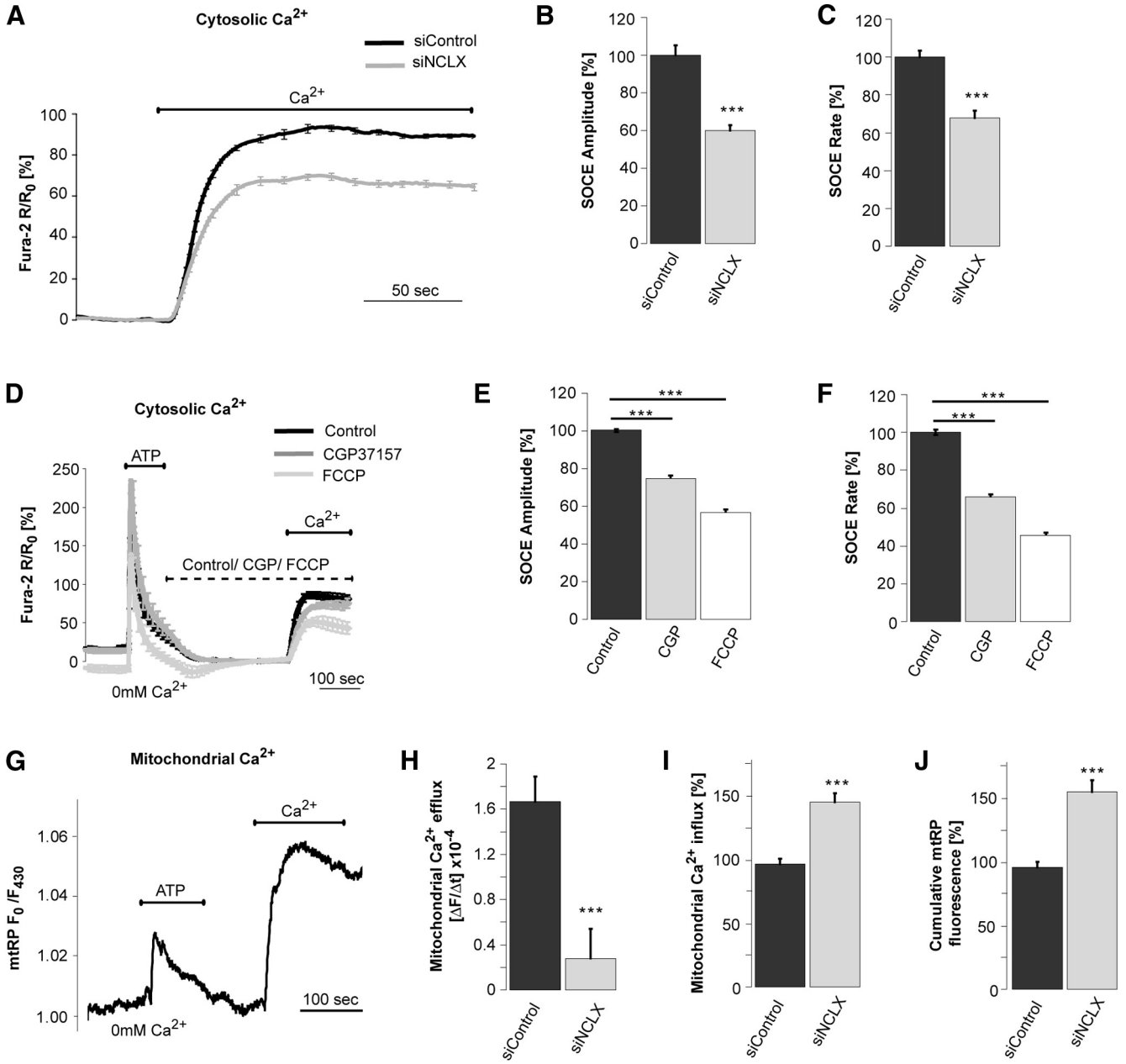

Figure 4. NCLX controls SOCE in astrocytes. ***A–C***, Imaging of cytosolic Ca^{2+} in fura-2 AM-loaded primary murine astrocytes. Astrocytes were cotransfected with siControl or siNCLX and siGLO red indicator. Cells were perfused in Ca^{2+}-free HEPES buffer and 100 μM ATP was applied to empty ER Ca^{2+} stores; then 5 mM Ca^{2+} was re-added as indicated by the bar to trigger the activation of SOCE. ***A***, Traces of average fura-2 AM fluorescence (normalized averages) during SOCE. ***B–C***, Amplitudes (***B***) and rates of SOCE (***C***) in siControl ($n = 9, n = 175$) and siNCLX-transfected astrocytes ($n = 9, n = 131$). Values are given as mean with SEM (***$p < 0.001$, Wilcoxon, Mann–Whitney *U* test). ***D–F***, Untransfected astrocytes were perfused in Ca^{2+}-free HEPES buffer without (Control) or with 20 μM CGP37157 or with 1 μM FCCP. After adding 100 μM ATP to empty the ER stores, 5 mM Ca^{2+} was added as indicated. ***D***, Mean Ca^{2+} response curve of all experiments (normalized averages). ***E–F***, Statistical analysis of the amplitudes (***E***) and SOCE rates (***F***) in astrocytes treated with CGP37157 (*CGP*), FCCP, or without any drug (Control). Values are given as mean with SEM summarized from $n = 8$ ($n = 376$ cells), $n = 7$ ($n = 425$ cells), and $n = 5$ ($n = 168$ cells) experiments for control, CGP37157, and FCCP-treated astrocytes, respectively (***$p < 0.001$, Kruskal-Wallis rank-sum test followed by Bonferoni's posttest and Wilcoxon test pair comparisons). ***G–J***, SOCE-induced mitochondrial Ca^{2+} signals in astrocytes cotransfected with mtRP and siControl or siNCLX using the same paradigm described in ***A***. ***G***, Representative curve showing the averaged mitochondrial Ca^{2+} response. ***H–J***, Rates of the mitochondrial Ca^{2+} efflux (***H***), influx (***I***), and cumulative fluorescence (***J***) from $n = 9$ experiments ($n = 59$ and $n = 43$ regions of interest for siControl- and siNCLX-transfected astrocytes, respectively; ***$p < 0.001$, Student's *t* test for unpaired samples and two-tailed and Mann–Whitney *U* test).

experiments, $n = 376$ and 425 cells for control and CGP37157-treated astrocytes, ***$p < 0.001$; Fig. 4*D–F*). Similarly, application of the protonophore FCCP, which leads to a collapse of membrane potential and a diminished calcium-buffering capacity of mitochondria, caused reductions in both the SOCE amplitude and rate (Fig. 4*D–F*). These results suggest that mitochondrial Ca^{2+} shuttling, and in particular NCLX activity, is of major importance for the regulation of Ca^{2+} influx into the cell through SOCE.

We next investigated whether Ca^{2+} influx via the SOCE pathway evokes mitochondrial Ca^{2+} transients and how NCLX activity regulates this cross talk. We adapted the Ca^{2+} re-admission protocol described above to mtRP-expressing astrocytes and determined mitochondrial Ca^{2+} transients. In this set of experiments, we measured only the wavelength F_{430} of the mtRP signal because ratiometric measurements of mtRP fluorescence F_{480}/F_{430} during SOCE for unknown reasons displayed a decrease in the signal-to-noise ratio. SOCE evoked a fast rise in mitochon-

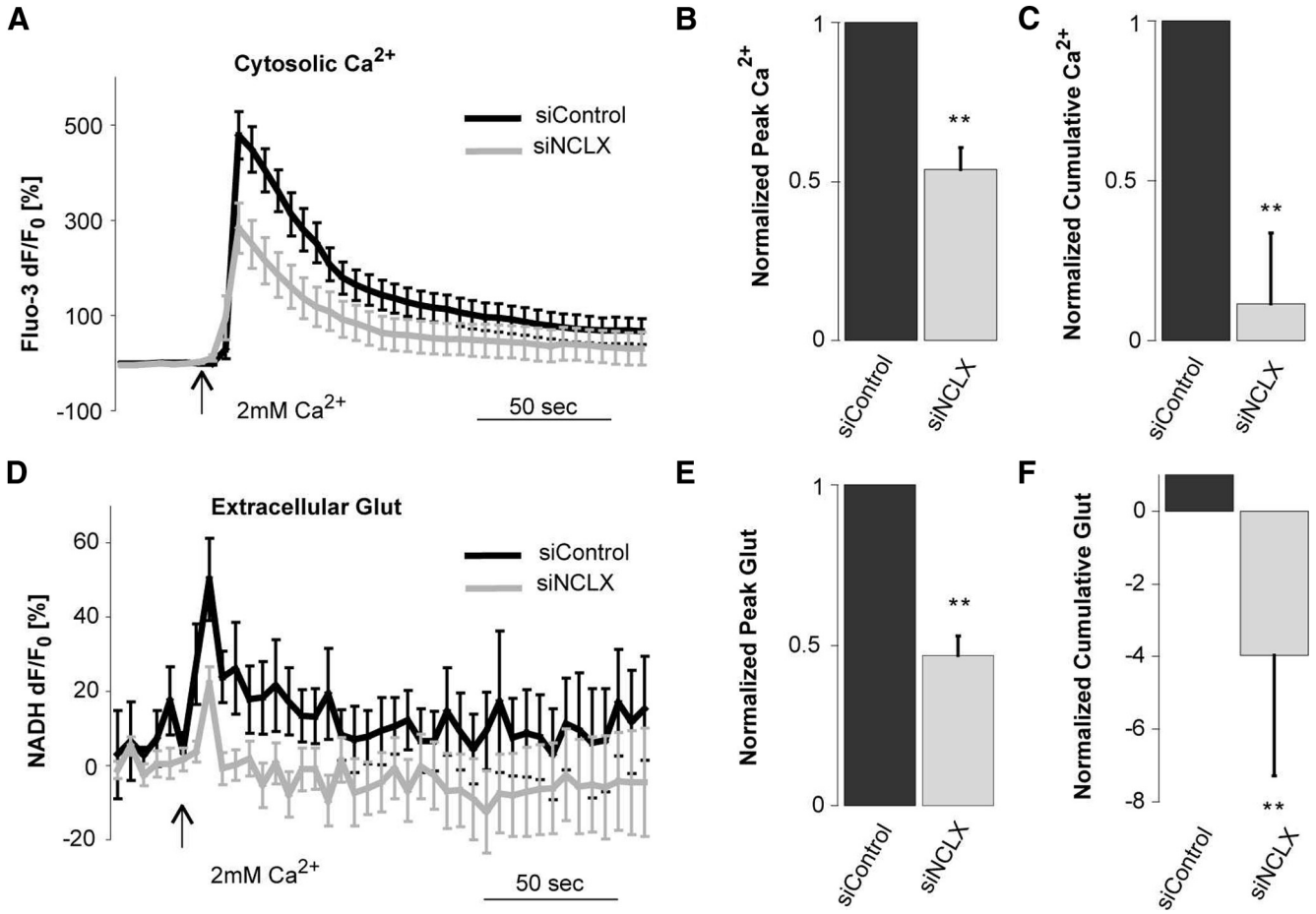

Figure 5. NCLX mediates increase of cytosolic Ca^{2+} and exocytotic glutamate release in astrocytes after mechanical stimulation. ***A–C***, Cytosolic Ca^{2+} measurements. ***A***, Time lapse of average fluo-3 AM fluorescence, reporting on changes in cytoplasmic Ca^{2+}, in solitary astrocytes transfected with either siControl or siNCLX in response to mechanical stimulation; all cells were cotransfected with the transfection marker siGLO. ***B***, Normalized fluo-3 AM peak. ***C***, Cumulative fluorescence values of mechanically stimulated solitary astrocytes in *A*. ***D–F***, Extracellular glutamate measurements. ***D***, Average kinetics of extracellular NADH fluorescence showing mechanically induced changes in extracellular glutamate surrounding somata of solitary astrocytes that were transfected as in ***A***. ***E***, ***F***, Normalized peak (***E***) and cumulative glutamate (Glut; ***F***) release from mechanically stimulated solitary astrocytes in ***D***. Solitary astrocytes transfected with siNCLX displayed significantly (Mann–Whitney *U* test, $^{**}p < 0.01$) reduced increase in mechanically induced Ca^{2+} signals and glutamate release compared with siControl-transfected cells. The points and bars represent means with SEMs of measurements from individual astrocytes ($n = 15$); Arrows in ***A*** and ***D*** represent the time when mechanical stimulation was applied to the cells.

drial Ca^{2+} signal followed by a gradual efflux (Fig. 4*G*). In NCLX-silenced astrocytes, mitochondrial Ca^{2+} efflux rate was clearly reduced compared with siControl-transfected cells ($1.67 \pm 0.22 \times 10^{-4}$/s and $0.28 \pm 0.26 \times 10^{-4}$/s, respectively, $n = 9$ experiments; $^{***}p < 0.001$; Fig. 4*H*). Concomitantly, upon activation of SOCE, the net influx of Ca^{2+} into the mitochondria was increased by 48.8% ($^{***}p < 0.001$; Fig. 4*I*) and the cumulative mitochondrial Ca^{2+} signal was elevated by 60.3% ($^{***}p < 0.001$; Fig. 4*J*) in NCLX-silenced astrocytes compared with the nonsilenced control.

These results indicate that an active cross talk exists between SOCE and mitochondria and that Ca^{2+} extrusion through NCLX is crucial for maintaining a strong SOCE activity in astrocytes.

NCLX- and Ca^{2+}-dependent glutamate release from astrocytes

To determine the impact of NCLX on Ca^{2+}-dependent functions of astrocytes, we studied the secretion of glutamate via the exocytotic/vesicular pathway induced by mechanical stimulation of astrocytes, which involves an increase of cytosolic Ca^{2+} (Innocenti et al., 2000; Hua et al., 2004; Montana et al., 2004). Mitochondria modulate the magnitude of this mechanically induced excitability (Reyes and Parpura, 2008). Interestingly, the pharmacological inhibitor of the mitochondrial Na^{+}/Ca^{2+} exchanger, CGP37157, has been shown previously to reduce mechanically induced Ca^{2+} responses and glutamate release from rat solitary astrocytes *in vitro* (Reyes and Parpura, 2008). In the present study, we assessed whether the molecular silencing of NCLX produced similar effects on astrocytic Ca^{2+} excitability and gliotransmission.

Astrocytes were transfected with the transfection marker siGLO, along with either siNCLX or a nontargeted siRNA in the control group and then loaded with fluo-3 AM to measure cytosolic Ca^{2+}. Similar to the purinergic receptor stimulation described above, mechanical stimulation caused an initial transient Ca^{2+} elevation ($n = 15$; peak $dF/F_0 = 478 \pm 43\%$; $^{**}p < 0.01$, paired *t* test) followed by a slowly decaying response in control solitary astrocytes transfected with the nontargeted siRNA (Fig. 5*A*). The transient peak was described to indicate the Ca^{2+} entry into the cytosol predominately from the ER store and from the extracellular space (Hua et al., 2004; Malarkey et al., 2008). Our data revealed a twofold decrease in both the peak ($n = 15$; peak $dF/F_0 = 283 \pm 52\%$) and a strong, fivefold decrease in cumulative cytosolic Ca^{2+} levels in siNCLX-treated cells ($^{**}p < 0.01$, Mann–Whitney *U* test; Fig. 5*A–C*). The knock-down of NCLX had a much larger inhibitory effect on the Ca^{2+} response than the

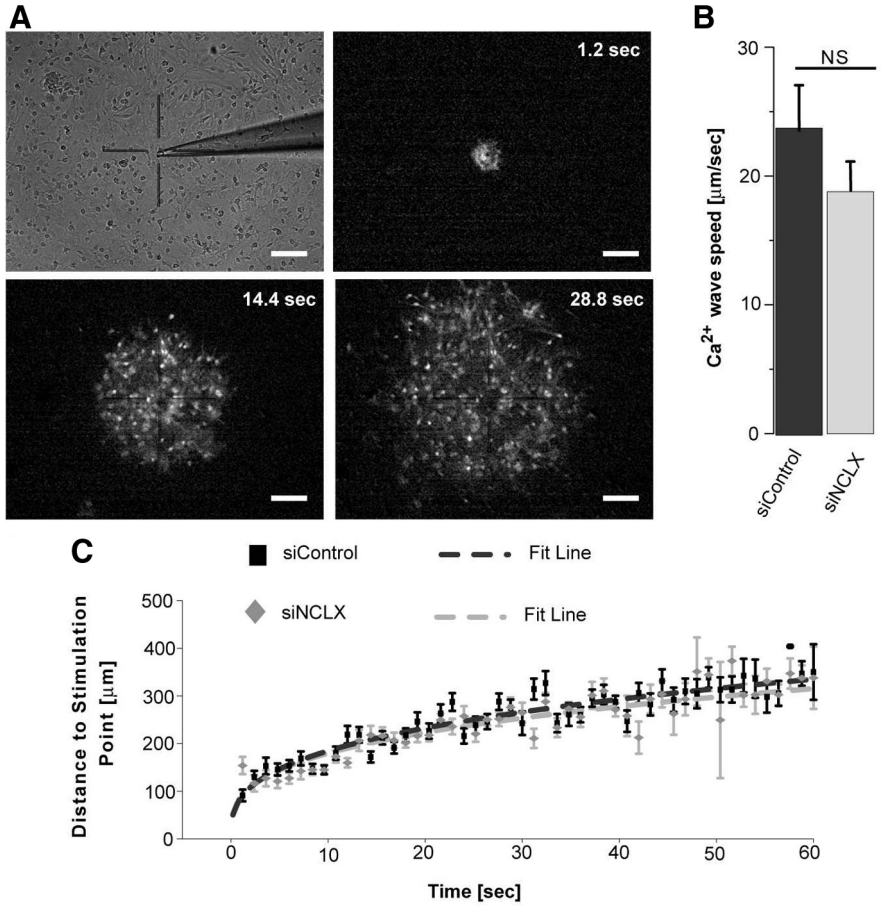

Figure 6. NCLX does not control the velocity of mechanically evoked Ca^{2+} waves in astrocytes. ***A***, Ca^{2+} waves were induced by mechanical stimulation in confluent astrocyte cultures, transfected with siControl or siNCLX, and loaded with fluo-4 AM to image cytosolic Ca^{2+}. ***A***, Series of subtraction images showing the concentric propagation of a Ca^{2+} wave as induced by poking an astrocyte with a micropipette (bright field image, top). ***B***, For each experiment, Ca^{2+} wave propagation velocity was calculated by averaging the velocities at which the Ca^{2+} wave reached each of the cells on a coverslip. (Wilcoxon, Mann–Whitney *U* test, $p > 0.05$, $n = 5$ astrocytic preparations, $n = 20$ and 28 coverslips for control and siNCLX, respectively). ***C***, Average time course of the propagation of the Ca^{2+} wave. The wave was initiated as a fast burst that propagated centrifugally close to a linear velocity. Mean data points could be fitted to a power function: distance $= A \times \text{time}^b$. For siControl-treated astrocytes, $A = 82 \pm 6.7$ μm and $b = 0.35 \pm 0.02$ ($R^2 = 0.92$), and for siNCLX-treated astrocytes, $A = 74 \pm 6.64$ μm and $b = 0.36 \pm 0.02$ ($R^2 = 0.82$). The values for *A* and *b* are given as mean ± SD. Values in the graph show mean ± SEM. Fitting curves are presented as dashed lines.

pharmacological inhibition of this exchanger by CGP37157, as described previously (Reyes and Parpura, 2008).

We next investigated the role of NCLX in Ca^{2+}-dependent exocytotic glutamate release from astrocytes. We used a GDH-linked assay based on accumulation of the fluorescent product NADH (Hua et al., 2004; Montana et al., 2004). Mechanical stimulation of the siControl-treated, solitary astrocytes evoked glutamate release, as indicated by a transient increase in NADH fluorescence ($n = 15$; peak $dF/F_0 = 50 \pm 11\%$; $^{**}p < 0.01$, paired *t* test; Fig. 5*D*), corresponding to glutamate surrounding the astrocytic somata. We observed a significant decrease in both normalized peak ($n = 15$; peak $dF/F_0 = 47 \pm 6\%$) and particularly in cumulative fluorescence intensity for glutamate release. After stimulation, basal levels of glutamate release was lower, when NCLX expression was knocked down when compared with the siControl group ($^{**}p < 0.01$, Mann–Whitney *U* test; Fig. 5*E*,*F*). These data indicate that NCLX plays an essential role in mediating cytosolic Ca^{2+} responses in astrocytes required for exocytotic glutamate gliotransmission.

Mechanically induced astrocytic Ca^{2+} waves are not affected by the activity of NCLX

Ca^{2+} waves in astrocyte networks constitute a form of intercellular communication and provide astrocytes with a specific form of excitability. In cultured astrocytes, Ca^{2+} signals can spread to neighboring cells and can propagate as a wave through many cells (Cornell-Bell et al., 1990; Dani et al., 1992; Schipke et al., 2002). Although different mechanisms have been described to account for the induction and maintenance of intercellular astroglial Ca^{2+} waves (Scemes and Giaume, 2006), there is nothing known so far on the role of mitochondria in the maintenance of the intercellullar astrocytic Ca^{2+} waves and whether Ca^{2+} efflux through NCLX contributes to the control of wave propagation in an astrocytic monolayer. We therefore measured velocities of Ca^{2+} waves in fluo-4 AM-loaded astrocytes that had been treated with siNCLX or control siRNA (Fig. 6*A*). An astrocyte within the monolayer was mechanically stimulated, as described above, and wave velocity was calculated for each cell by an algorithm that measures the distance from the stimulation point and the time at which the wave reached a given cell. Although the averaged velocity of the Ca^{2+} wave was 23.9 ± 3.3 μm/s for siControl astrocytes, and 18.8 ± 2.3 μm/s on average for the NCLX-silenced astrocytes, it was not significantly different (Fig. 6*B*). A wave was initiated as a rapid onset, followed by centrifugal propagation with almost linear velocity. The averaged time course of the waves is shown in Figure 6*C*. The mean data points were fitted to the following power functions: in siControl-treated astrocytes, distance $= 82 \pm 6.7 \times \text{time}^{0.35 \pm 0.02}$, $R^2 = 0.92$, and in NCLX-treated astrocytes, distance $= 74 \pm 6.6 \times \text{time}^{0.36 \pm 0.02}$, $R^2 = 0.82$). The slight reduction in the Ca^{2+} wave velocity that we observed in NCLX-silenced astrocytes was not significant, which suggests that the activity of the mitochondrial exchanger only marginally, if at all, affects the Ca^{2+} signaling machinery contributing to propagation of intercellular Ca^{2+} waves in astrocytes.

NCLX participates in control of astrocytic wound healing *in vitro*

Astrocyte migration and proliferation represent important cellular aspects of the brain's response to injury and during regeneration. Intracellular Ca^{2+} signaling is critical to the regulation of these cellular responses (Xu et al., 2004; Valero et al., 2008; Wei et al., 2009; Feldman et al., 2010). Therefore, we investigated whether the mitochondrial Na^+/Ca^{2+} exchanger NCLX affects these functional parameters in astrocytes.

To assess the effect of NCLX on astrocytic wound healing, we adapted an *in vitro* assay described previously (Környei et al., 2000; Matyash et al., 2002). Monolayers of astrocytes that had

either been treated with NCLX siRNA or with control siRNA, as well as mock-transfected and untreated astrocytes, were scratched as indicated in Figure 7*B* and the cell-free area was measured immediately after scratching as described by Gebäck et al. (2009) (Fig. 7*A*). Thereafter, repopulation was analyzed repeatedly 48–72 h after scratching until the wound area was closed by at least two-thirds in the untreated control (end point). Molecular silencing of NCLX with siRNA significantly impaired the astrocytic ability to repopulate the cell-free area (Fig. 7*B*,*C*). Although the scratch was closed by more than two-thirds after 48–72 h in siControl cultures, it remained much larger when NCLX was inhibited: the mean open wound area in NCLX-silenced astrocytes was 48.5 ± 2.6% on average compared with 24.6 ± 2.5% for the siControl conditions ($n = 3$ experiments, $n = 20$ scratches, $^{***}p < 0.001$; Fig. 7*C*), and these observations were confirmed in cultures treated with 20 μm CGP37157 throughout the regrowth phase (data not shown), indicating that NCLX activity is crucial for astrocytic migration and wound closure *in vitro*.

To assess whether NCLX exerts an effect on astrocyte proliferation, we performed cell proliferation assays based on BrdU incorporation in noninjured cultures. Astrocyte proliferation was decreased by 38.6% in NCLX-silenced astrocyte cultures compared with astrocytes transfected with nontargeted siRNA (siControl, $n = 3$ experiments, $n = 15$ wells, $^{***}p < 0.001$; Fig. 7*D*). A possible harmful side effect of the transfection procedure can be excluded because the proliferation in the siControl and mock-transfected cultures was not impaired compared with the untreated control astrocytes.

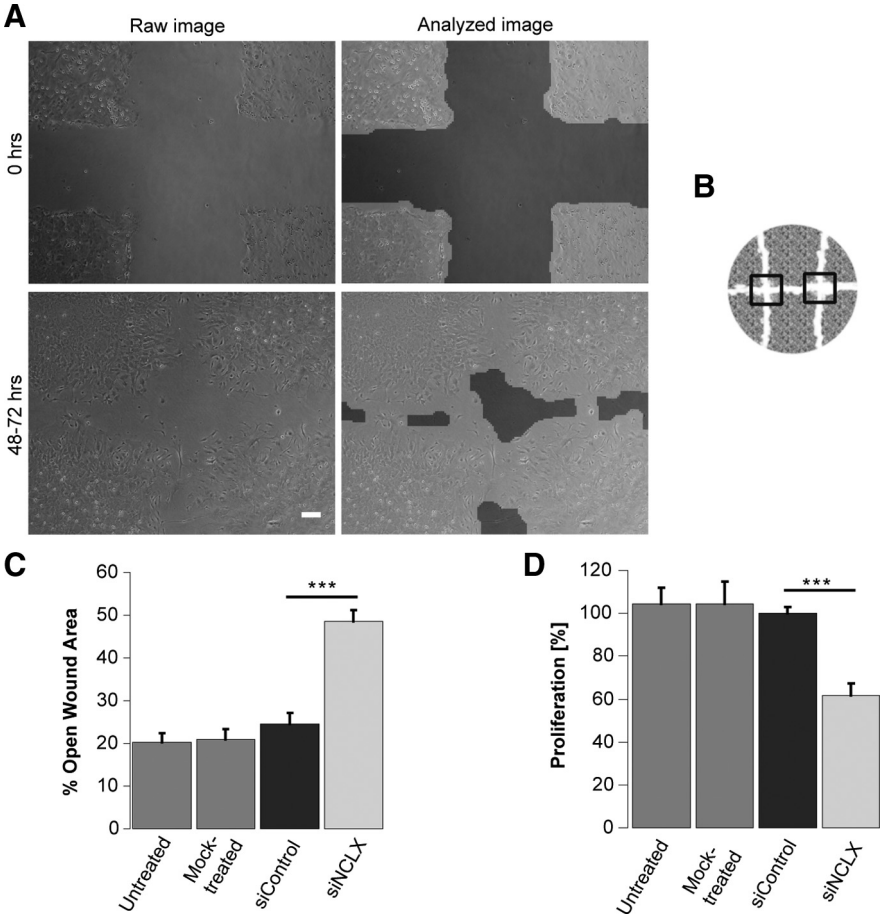

Figure 7. NCLX participates in astrocytic *in vitro* wound healing and proliferation. ***A***, Confluent astrocytic monolayers were scratched as described in the Materials and Methods, and phase contrast images were acquired at 0 h (top row) and after 48–72 h (bottom row) at low magnification. Left column shows raw images and right column shows the same images after analysis with T-scratch software. Dark gray areas correspond to the open wound area; values at the end point are normalized to a 100% area at the starting point (0 h). Scale bar, 100 μm. ***B***, Scheme exemplifying how scratches (white lines) were applied to astrocyte monolayers (gray areas). Black frames correspond to the analyzed areas of interest. ***C***, Percentage of open wound area in monolayers that were untransfected, mock-transfected, or transfected with siControl or siNCLX ($n = 3$ cultures, $n = 18$, 16, 20, and 20 scratches, respectively). Values are given as means with SEM ($^{***}p < 0.001$, Student's *t* test for unpaired samples, two-tailed). ***D***, BrdU incorporation into proliferating astrocytes that were untransfected, mock-transfected, or transfected with siControl or siNCLX, given as percentage proliferation normalized to control ($n = 3$ experiments, $n = 15$ wells; $^{***}p < 0.001$, Mann–Whitney *U* test).

These findings indicate that the mitochondrial Na^+/Ca^{2+} exchanger NCLX is involved in the control of astrocytic wound closure and proliferation.

Discussion

Mitochondria are critically involved in Ca^{2+} handling in astrocytes, thereby modifying astrocytic functions (Verkhratsky et al., 2012). In the present study, we addressed the specific role of NCLX in shaping astrocytic mitochondrial and cytoplasmic Ca^{2+} signals and studied its impact on Ca^{2+}-dependent astrocyte functions. We show that NCLX, which is enriched in astrocytic mitochondria, mediates Ca^{2+} extrusion from mitochondria. In addition, NCLX predominately modulated the SOCE pathway, whereas its effect on the ER-dependent Ca^{2+} release was minor. Therefore, NCLX activity has a major impact on modulating cytoplasmic Ca^{2+} signals in astrocytes, as well as their functional output, exocytotic glutamate release, wound closure, and proliferation, but does not significantly influence the propagation of mechanically induced Ca^{2+} waves in astrocytic monolayers.

Our immunochemical approach verified that the NCLX protein is expressed in astrocytes and occurs as an ~60 kDa and an ~100 kDa form that is consistently related to an SDS-resistant NCLX dimer (Palty et al., 2004; Palty et al., 2006). Comparison of NCLX expression in different organelle-enriched fractions of astrocytes revealed a strong enrichment of NCLX in the mitochondria, indicating that it is primarily located in these organelles. The MW of mitochondrial NCLX, interestingly, was slightly reduced to ~50 kDa compared with the other cellular compartments. Although the physiological role of such processing is not yet clear and we cannot rule out whether NCLX cleavage occurred during mitochondrial isolation, the reduction in MW is consistent with the sensitivity of NCLX to mitochondrial proteases such as mitochondrial calpains (Kar et al., 2009; Smith and Schnellmann, 2012). Alternatively, because our antibody is targeted to the C-terminal domain of NCLX, cleavage is likely to occur on the NH3-terminal NCLX domains. The *N*-terminal domains usually harbor the mitochondria-targeting peptide that can be cleaved during mitochondrial insertion (Moss-

mann et al., 2012). Although these mechanisms need to be investigated further, they raise interesting questions regarding posttranslational regulation of NCLX in mitochondria.

NCLX modulates glial Ca^{2+} signaling

An important finding of our study is that NCLX activity promotes SOCE in astrocytes. Sustained Ca^{2+} influx through SOCE results in prolonged intracellular Ca^{2+} transients that are particularly important in controlling slow cellular processes such as secretory activity and cell proliferation (Hoth et al., 1997; Golovina, 1999; Golovina et al., 2001; Berridge et al., 2003).

Several studies have documented a pivotal role of the mitochondrial exchanger in the replenishment of the ER Ca^{2+} stores (Arnaudeau et al., 2001; Malli et al., 2005; Kim et al., 2012). We found that ER Ca^{2+} release, which can be considered an indicative value for ER Ca^{2+} content, was not much altered by the knock-down of NCLX expression. Although the molecular basis for this relatively minor influence of NCLX on ER Ca^{2+} needs to be explored further, it may be related to the major role of SERCA in refilling the astrocytic Ca^{2+} stores, even under NCLX deficiency. In addition, transfer of Ca^{2+} from the mitochondria to the ER Ca^{2+} stores is facilitated by the tight physical interactions mediated by an ER–mitochondria-tethering protein complex and direct Ca^{2+} transport through these compartments via the voltage-dependent anion channels (Szabadkai et al., 2006; Kornmann et al., 2009; de Brito and Scorrano, 2010). Our results suggest that such cross talk between the the ER and mitochondria is relatively weak in astrocytes. This assertion is consistent with our findings that the strong cytosolic Ca^{2+} response triggered by ER Ca^{2+} release was followed by only a modest mitochondrial Ca^{2+} transient compared with a much stronger mitochondrial Ca^{2+} transient triggered by Ca^{2+} influx into the cells. The latter effect suggests a stronger interaction of NCLX with the SOCE pathway. It is not surprising that astrocytic intracellular Ca^{2+} dynamics are inherently linked to those of Na^+ (Kirischuk et al., 2012). Therefore, in addition to obvious exchange of these ions via NCLX, cytoplasmic Na^+ concentrations would also be affected by diverse plasma membrane receptors and transporters involved in Na^+ exchange, among them SOCE and/or P2XRs, and the cytosolic Na^+ load thus affects a multitude of astroglial homeostatic functions (Kirischuk et al., 2012).

Mitochondrial metabolism is likely to be affected by the activity of NCLX, because Ca^{2+} activates several enzymes of the Krebs cycle (Szabadkai and Duchen, 2008). NCLX, by accelerating mitochondrial Ca^{2+} shuttling, increases the duration of mitochondrial Ca^{2+} transients and thereby is likely to enhance ATP production.

NCLX activity differentially affects migration/proliferation

We used an *in vitro* model to study the impact of NCLX function on the ability of astrocytes to populate a cell-free area as a model for wound healing. The repopulation of the cell-free "wound" area is primarily due to astrocyte proliferation, although migration does also contribute to this process (Környei et al., 2000). A role of SOCE in wound closure has been proposed previously (Rao et al., 2006). Our study strongly suggests that mitochondrial Ca^{2+} transfer through NCLX is essential to facilitate SOCE, and therefore may affect astrocytic proliferation and the regrowth of the astrocytes into the denuded areas of the wound. Although the downstream mitogenic signaling pathways that link the Ca^{2+} response to migration and proliferation still need to be investigated, earlier studies have highlighted the role of the mitochondrial exchanger in activating the PI3 kinase pathway by accelerating SOCE-related cellular Ca^{2+} rise (Feldman et al., 2010).

NCLX activity does not affect astrocytic Ca^{2+} wave propagation

Propagating Ca^{2+} waves are a major communication pathway of the astrocytic network and of neuron–astrocyte communication. Different mechanisms account for the induction and maintenance of intercellular astroglial Ca^{2+} waves. These involve the release of gliotransmitters, as well as direct diffusion of $InsP_3$ through gap junctions into neighboring astrocytes, where it activates $InsP_3$ receptors and subsequent release of Ca^{2+} from ER stores (Scemes and Giaume, 2006). On a single-cell level (intracellular Ca^{2+} waves), mitochondrial Ca^{2+} buffering has been described as an important means to attenuate excess Ca^{2+} levels at the $InsP_3R$ microdomains (Boitier et al., 1999) to keep the amplification working. However, little is known about the role of mitochondria in the maintenance of the intercellullar astrocytic Ca^{2+} waves and whether Ca^{2+} efflux through NCLX contributes to the control of wave propagation in an astrocytic monolayer. Our results show that the knock-down of NCLX does not induce a significant change in astrocyte Ca^{2+} wave propagation velocity. The less dominant role of the mitochondrial exchanger in wave propagation may be related to at least two issues. First, the rates of mitochondrial Ca^{2+} uptake are approximately two orders of magnitude faster than mitochondrial Ca^{2+} efflux, which spans over tens of seconds (Fig. 2*C*; Palty et al., 2010). However, the propagation of the cytosolic astrocytic Ca^{2+} wave is much more rapid, thus crossing a single glial cell within less than a second. At this rate, the contribution of the slower mitochondrial exchanger to cytosolic Ca^{2+} is predicted to be minimal. Second, in addition, Ca^{2+} release from the ER is the dominant pathway providing Ca^{2+} during wave propagation. Because ER Ca^{2+} release is not strongly affected by the knock-down of NCLX, it is thus less likely to play a dominant role in propagation of the Ca^{2+} wave.

NCLX is instrumental in increasing cytosolic Ca^{2+} for triggering release of gliotransmitter glutamate

Previous work used a pharmacological approach to assess the role of the mitochondrial Na^+/Ca^{2+} exchanger in cytoplasmic Ca^{2+} dynamics in astrocytes: inhibition by CGP37157 resulted in a reduction of mechanically induced Ca^{2+} responses and glutamate release recorded from cultured rat solitary astrocytes (Reyes and Parpura, 2008). The molecular identification of NCLX (Palty et al., 2010) now provides a more specific, siRNA-based molecular tool with which to study its role on mechanically induced Ca^{2+} responses and glutamate release from astrocytes. Although our data are consistent with previous pharmacological data, they provide new insight on the role of the exchanger. Most notably, the molecular knock-down of NCLX triggered a more profound inhibitory effect on mechanically induced increase of cytosolic $Ca^{2+}$and subsequent exocytotic release of glutamate than the pharmacological approach (Reyes and Parpura, 2008). The reason for the differences between the acute pharmacological versus the siRNA approach could be the multiple sites of CGP37157 action, among them Ca^{2+} transporters. The molecular knock-down approach is specific for NCLX, whereas the pharmacological approach may partially mask the full effect of the mitochondrial exchanger on glutamate secretion due to side effects on other transport molecules. Because vesicular glutamate transporter 3 and cytoplasmic glutamate levels in astrocytes regulate the magnitude of exocytotic glutamate release from astrocytes (Ni and Parpura, 2009), a possible explanation for

unparalleled changes in cytoplasmic Ca^{2+} and Ca^{2+}-dependent glutamate release could be that astrocytes lacking NCLX have less glutamate available for vesicular storage and release. *De novo* glutamate synthesis relies on the mitochondrial matrix enzyme pyruvate carboxylase (Hertz et al., 1999), which is activated by Ca^{2+}(Civelek et al., 1996). However, our observation that the knock-down of NCLX results in a sustained increase, rather than a decrease, in mitochondrial free Ca^{2+} would not support such a scenario. Therefore, it is tempting to hypothesize that NCLX, by modulation of glutamate release from astrocytes, has a role in synaptic transmission and plasticity at the tripartite synapse.

References

Agulhon C, Petravicz J, McMullen AB, Sweger EJ, Minton SK, Taves SR, Casper KB, Fiacco TA, McCarthy KD (2008) What is the role of astrocyte calcium in neurophysiology? Neuron 59:932–946. CrossRef Medline

Arnaudeau, S, Kelley WL, Walsh JV, Jr, and Demaurex N. (2001) Mitochondria recycle Ca(2+) to the endoplasmic reticulum and prevent the depletion of neighboring endoplasmic reticulum regions. J Biol Chem 276:29430–29439.

Baughman JM, Perocchi F, Girgis HS, Plovanich M, Belcher-Timme CA, Sancak Y, Bao XR, Strittmatter L, Goldberger O, Bogorad RL, Koteliansky V, Mootha VK (2011) Integrative genomics identifies MCU as an essential component of the mitochondrial calcium uniporter. Nature 476:341–345. CrossRef Medline

Bernardinelli Y, Azarias G, Chatton JY (2006) In situ fluorescence imaging of glutamate-evoked mitochondrial Na+ responses in astrocytes. Glia 54:460–470. CrossRef Medline

Berridge MJ, Bootman MD, Roderick HL (2003) Calcium signalling: dynamics, homeostasis and remodelling. Nat Rev Mol Cell Biol 4:517–529. CrossRef Medline

Boitier E, Rea R, Duchen MR (1999) Mitochondria exert a negative feedback on the propagation of intracellular Ca2+ waves in rat cortical astrocytes. J Cell Biol 145:795–808. CrossRef Medline

Bozidis P, Williamson CD, Colberg-Poley AM. (2007) Isolation of endoplasmic reticulum, mitochondria, and mitochondria-associated membrane fractions from transfected cells and from human cytomegalovirus-infected primary fibroblasts. Curr Protoc Cell Biol. Chapter 3:Unit 3.27. CrossRef Medline

Civelek VN, Deeney JT, Shalosky NJ, Tornheim K, Hansford RG, Prentki M, Corkey BE (1996) Regulation of pancreatic beta-cell mitochondrial metabolism: influence of Ca2+, substrate and ADP. Biochem J 318:615–621. Medline

Contreras L, Drago I, Zampese E, Pozzan T (2010) Mitochondria: the calcium connection. Biochim Biophys Acta 1797:607–618. CrossRef Medline

Cornell-Bell AH, Finkbeiner SM, Cooper MS, Smith SJ (1990) Glutamate induces calcium waves in cultured astrocytes: long-range glial signaling. Science 247:470–473. CrossRef Medline

Czyz A, Kiedrowski L (2003) Inhibition of plasmalemmal Na(+)/Ca(2+) exchange by mitochondrial Na(+)/Ca(2+) exchange inhibitor 7-chloro-5-(2-chlorophenyl)-1,5-dihydro-4,1-benzothiazepin-2(^{3}H)-one (CGP-37157) in cerebellar granule cells. Biochem Pharmacol 66:2409–2411. CrossRef Medline

Dani JW, Chernjavsky A, Smith SJ (1992) Neuronal activity triggers calcium waves in hippocampal astrocyte networks. Neuron 8:429–440. CrossRef Medline

de Brito OM, Scorrano L (2010) An intimate liaison: spatial organization of the endoplasmic reticulum-mitochondria relationship. EMBO J 29:2715–2723. CrossRef Medline

De Stefani D, Raffaello A, Teardo E, Szabò I, Rizzuto R (2011) A forty-kilodalton protein of the inner membrane is the mitochondrial calcium uniporter. Nature 476:336–340. CrossRef Medline

Drago I, Pizzo P, and Pozzan T. (2011) After half a century mitochondrial calcium in- and efflux machineries reveal themselves. EMBO J 30:4119–4125. CrossRef Medline

Feldman B, Fedida-Metula S, Nita J, Sekler I, Fishman D (2010) Coupling of mitochondria to store-operated Ca(2+)-signaling sustains constitutive activation of protein kinase B/Akt and augments survival of malignant melanoma cells. Cell Calcium 47:525–537. CrossRef Medline

Gebäck T, Schulz MM, Koumoutsakos P, Detmar M (2009) TScratch: a novel and simple software tool for automated analysis of monolayer wound healing assays. Biotechniques 46:265–274. CrossRef Medline

Golovina VA (1999) Cell proliferation is associated with enhanced capacitative Ca(2+) entry in human arterial myocytes. Am J Physiol 277:C343–349. Medline

Golovina VA, Platoshyn O, Bailey CL, Wang J, Limsuwan A, Sweeney M, Rubin LJ, Yuan JX (2001) Upregulated TRP and enhanced capacitative Ca^{2+} entry in human pulmonary artery myocytes during proliferation. Am J Physiol Heart Circ Physiol 280:H746–H755. Medline

Hajnóczky G, Hager R, Thomas AP (1999) Mitochondria suppress local feedback activation of inositol 1,4, 5-trisphosphate receptors by Ca^{2+}. J Biol Chem 274:14157–14162. CrossRef Medline

Hertz L, Dringen R, Schousboe A, Robinson SR (1999) Astrocytes: glutamate producers for neurons. J Neurosci Res 57:417–428. CrossRef Medline

Hoth M, Fanger CM, Lewis RS (1997) Mitochondrial regulation of store-operated calcium signaling in T lymphocytes. J Cell Biol 137:633–648. CrossRef Medline

Hua X, Malarkey EB, Sunjara V, Rosenwald SE, Li WH, Parpura V (2004) Ca2+-dependent glutamate release involves two classes of endoplasmic reticulum Ca2+ stores in astrocytes. J Neurosci Res 76:86–97. CrossRef Medline

Innocenti B, Parpura V, Haydon PG (2000) Imaging extracellular waves of glutamate during calcium signaling in cultured astrocytes. J Neurosci 20:1800–1808. Medline

Jiang D, Zhao L, Clapham DE (2009) Genome-wide RNAi screen identifies Letm1 as a mitochondrial Ca2+/H+ antiporter. Science 326:144–147. CrossRef Medline

Kann O, Kovács R (2007) Mitochondria and neuronal activity. Am J Physiol Cell Physiol 292:C641–657. CrossRef Medline

Kar P, Chakraborti T, Samanta K, Chakraborti S (2009) mu-Calpain mediated cleavage of the Na+/Ca2+ exchanger in isolated mitochondria under A23187 induced Ca2+ stimulation. Arch Biochem Biophys 482:66–76. CrossRef Medline

Kim B, Takeuchi A, Koga O, Hikida M, Matsuoka S (2012a) Pivotal role of mitochondrial Na^+-Ca^{2+} exchange in antigen receptor mediated Ca^{2+} signalling in DT40 and A20 B lymphocytes. J Physiol 590:459–474. CrossRef Medline

Kirischuk S, Parpura V, Verkhratsky A (2012) Sodium dynamics: another key to astroglial excitablity? Trends Neurosci 35:497–506. CrossRef Medline

Kornmann B, Currie E, Collins SR, Schuldiner M, Nunnari J, Weissman JS, Walter P (2009) An ER-mitochondria tethering complex revealed by a synthetic biology screen. Science 325:477–481. CrossRef Medline

Környei Z, Czirók A, Vicsek T, Madarász E (2000) Proliferative and migratory responses of astrocytes to *in vitro* injury. J Neurosci Res 61:421–429. CrossRef Medline

Kresse W, Sekler I, Hoffmann A, Peters O, Nolte C, Moran A, Kettenmann H (2005) Zinc ions are endogenous modulators of neurotransmitter-stimulated capacitative Ca2+ entry in both cultured and in situ mouse astrocytes. Eur J Neurosci 21:1626–1634. CrossRef Medline

Lee W, Malarkey EB, Reyes RC, Parpura V (2008) Micropit: a new cell culturing approach for characterization of solitary astrocytes and small networks of these glial cells. Front Neuroeng 2008;1:2. CrossRef Medline

Lyons SA, Kettenmann H (1998) Oligodendrocytes and microglia are selectively vulnerable to combined hypoxia and hypoglycemia injury *in vitro*. J Cereb Blood Flow Metab 18:521–530. CrossRef Medline

Malarkey EB, Parpura V (2011) Temporal characteristics of vesicular fusion in astrocytes: examination of synaptobrevin 2-laden vesicles at single vesicle resolution. J Physiol 589:4271–4300. CrossRef Medline

Malarkey EB, Ni Y, Parpura V (2008) Ca2+ entry through TRPC1 channels contributes to intracellular Ca2+ dynamics and consequent glutamate release from rat astrocytes. Glia 56:821–835. CrossRef Medline

Malli R, Frieden M, Osibow K, Zoratti C, Mayer M, Demaurex N, Graier WF (2003) Sustained Ca2+ transfer across mitochondria is Essential for mitochondrial Ca2+ buffering, sore-operated Ca2+ entry, and Ca2+ store refilling. J Biol Chem 278:44769–44779. CrossRef Medline

Malli R, Frieden M, Trenker M, Graier WF (2005) The role of mitochondria for Ca2+ refilling of the endoplasmic reticulum. J Biol Chem 280:12114–12122. CrossRef Medline

Matyash M, Matyash V, Nolte C, Sorrentino V, Kettenmann H (2002) Re-

quirement of functional ryanodine receptor type 3 for astrocyte migration. FASEB J 16:84–86. CrossRef Medline
Montana V, Ni Y, Sunjara V, Hua X, Parpura V (2004) Vesicular glutamate transporter-dependent glutamate release from astrocytes. J Neurosci 24:2633–2642. CrossRef Medline
Mossmann D, Meisinger C, Vögtle FN (2012) Processing of mitochondrial presequences. Biochim Biophys Acta 1819:1098–1106. CrossRef Medline
Nagai T, Sawano A, Park ES, Miyawaki A (2001) Circularly permuted green fluorescent proteins engineered to sense Ca2+. Proc Natl Acad Sci U S A 98:3197–3202. CrossRef Medline
Neumann JT, Diaz-Sylvester PL, Fleischer S, Copello JA (2011) CGP-37157 inhibits the sarcoplasmic reticulum Ca(2)+ ATPase and activates ryanodine receptor channels in striated muscle. Mol Pharmacol 79:141–147. CrossRef Medline
Ni Y, Parpura V (2009) Dual regulation of Ca2+-dependent glutamate release from astrocytes: vesicular glutamate transporters and cytosolic glutamate levels. Glia 57:1296–1305. CrossRef Medline
Palty R, Ohana E, Hershfinkel M, Volokita M, Elgazar V, Beharier O, Silverman WF, Argaman M, Sekler I (2004) Lithium-calcium exchange is mediated by a distinct potassium-independent sodium-calcium exchanger. J Biol Chem 279:25234–25240. CrossRef Medline
Palty R, Hershfinkel M, Yagev O, Saar D, Barkalifa R, Khananshvili D, Peretz A, Grossman Y, Sekler I (2006) Single alpha-domain constructs of the Na+/Ca2+ exchanger, NCLX, oligomerize to form a functional exchanger. Biochemistry 45:11856–11866. CrossRef Medline
Palty R, Silverman WF, Hershfinkel M, Caporale T, Sensi SL, Parnis J, Nolte C, Fishman D, Shoshan-Barmatz V, Herrmann S, Khananshvili D, Sekler I (2010) NCLX is an essential component of mitochondrial Na+/Ca2+ exchange. Proc Natl Acad Sci U S A 107:436–441. CrossRef Medline
Parekh AB (2008) Mitochondrial regulation of store-operated CRAC channels. Cell Calcium 44:6–13. CrossRef Medline
Perea G, Navarrete M, Araque A (2009) Tripartite synapses: astrocytes process and control synaptic information. Trends Neurosci 32:421–431. CrossRef Medline
Pivneva T, Haas B, Reyes-Haro D, Laube G, Veh RW, Nolte C, Skibo G, Kettenmann H (2008) Store-operated Ca2+ entry in astrocytes: different spatial arrangement of endoplasmic reticulum explains functional diversity *in vitro* and in situ. Cell Calcium 43:591–601. CrossRef Medline
Pizzo P, Drago I, Filadi R, Pozzan T (2012) Mitochondrial Ca(2+) homeostasis: mechanism, role, and tissue specificities. Pflugers Arch 464:3–17. CrossRef Medline
Rao JN, Platoshyn O, Golovina VA, Liu L, Zou T, Marasa BS, Turner DJ, Yuan JX, Wang JY (2006) TRPC1 functions as a store-operated Ca2+ channel in intestinal epithelial cells and regulates early mucosal restitution after wounding. Am J Physiol Gastrointest Liver Physiol 290:G782–G792. CrossRef Medline
Reyes RC, Parpura V (2008) Mitochondria modulate Ca2+-dependent glutamate release from rat cortical astrocytes. J Neurosci 28:9682–9691. CrossRef Medline
Reyes RC, Perry G, Lesort M, Parpura V (2011) Immunophilin deficiency augments Ca2+-dependent glutamate release from mouse cortical astrocytes. Cell Calcium 49:23–34. CrossRef Medline
Scemes E, Giaume C (2006) Astrocyte calcium waves: what they are and what they do. Glia 54:716–725. CrossRef Medline
Schipke CG, Boucsein C, Ohlemeyer C, Kirchhoff F, Kettenmann H (2002) Astrocyte Ca2+ waves trigger responses in microglial cells in brain slices. FASEB J 16:255–257. CrossRef Medline
Shapiro LG, Stockman GC (2001) Computer vision. Upper Saddle River, NJ: Prentice Hall.
Smith MA, Schnellmann RG (2012) Calpains, mitochondria, and apoptosis. Cardiovasc Res 96:32–37. CrossRef Medline
Szabadkai G, Duchen MR (2008) Mitochondria: the hub of cellular Ca2+ signaling. Physiology (Bethesda) 23:84–94. CrossRef Medline
Szabadkai G, Simoni AM, Bianchi K, De Stefani D, Leo S, Wieckowski MR, Rizzuto R (2006) Mitochondrial dynamics and Ca2+ signaling. Biochim Biophys Acta 1763:442–449. CrossRef Medline
Thu le T, Ahn JR, Woo SH (2006) Inhibition of L-type Ca2+ channel by mitochondrial Na+-Ca2+ exchange inhibitor CGP-37157 in rat atrial myocytes. Eur J Pharmacol 552:15–19. CrossRef Medline
Valero RA, Senovilla L, Núñez L, Villalobos C (2008) The role of mitochondrial potential in control of calcium signals involved in cell proliferation. Cell Calcium 44:259–269. CrossRef Medline
Verkhratsky A, Rodríguez JJ, Parpura V (2012) Calcium signalling in astroglia. Mol Cell Endocrinol 353:45–56. CrossRef Medline
Wei C, Wang X, Chen M, Ouyang K, Song LS, Cheng H (2009) Calcium flickers steer cell migration. Nature 457:901–905. CrossRef Medline
Xu HT, Yuan XB, Guan CB, Duan S, Wu CP, Feng L (2004) Calcium signaling in chemorepellant Slit2-dependent regulation of neuronal migration. Proc Natl Acad Sci U S A 101:4296–4301. CrossRef Medline
Zack GW, Rogers WE, Latt SA (1977) Automatic measurement of sister chromatid exchange frequency. J Histochem Cytochem 25:741–753. CrossRef Medline